https://doi.org/10.5194/bg-2020-435
Preprint. Discussion started: 6 January 2021

Biogeosciences Discussions

Advancing on large-scale trends of apparent organic matter reactivity in marine sediments and patterns of benthic carbon transformation

Felipe S. Freitas[1,3†], Philip A. Pika[2,4††], Sabine Kasten[5,6,7], Bo B. Jørgensen[8], Jens Rassmann[9], Christophe Rabouille[9], Shaun Thomas[10, †††], Henrik Sass[10], Richard D. Pancost[1,3], Sandra Arndt[4]

[1]Organic Geochemistry Unit, School of Earth Sciences & School of Chemistry, University of Bristol, Bristol, BS8 1TS, United Kingdom
[2]BRIDGE, School of Geographical Sciences, University of Bristol, Bristol, BS8 1RL, United Kingdom
[3]Cabot Institute for the Environment, University of Bristol, Bristol, BS8 1UH, United Kingdom
[4]Biogeochemistry and Earth System Modeling, Geosciences, Environment and Society Department, Université Libre de Bruxelles, Brussels, CP160/03 1050, Belgium
[5]Alfred Wegener Institute Helmholtz Centre for Polar and Marine Research, Bremerhaven, 27570, Germany
[6]Faculty of Geosciences, University of Bremen, 28359 Bremen, Germany
[7]MARUM – Center for Marine Environmental Sciences, University of Bremen, 28359 Bremen, Germany
[8]Section for Microbiology, Department of Biology, Aarhus University, 8000 Aarhus C, Denmark
[9]Laboratoire des Sciences du Climat et de l'Environnement, LSCE/IPSL, CEA-CNRS-UVSQ-Université Paris Saclay, 91198 Gif-sur-Yvette, France
[10]School of Earth and Ocean Sciences, Cardiff University, Cardiff, CF10 3AT, United Kingdom

[†] Current address: School of Earth Sciences, University of Bristol, Bristol, BS8 1RJ, United Kingdom
[††] Current address: Department of Earth Sciences, VU University of Amsterdam, 1081 HV Amsterdam, The Netherlands
[†††] Current address: RSR Ltd, Parc Ty Glas, Llanishen, Cardiff, CF14 5DU, United Kingdom

Correspondence to: Felipe S. Freitas (felipe.salesdefreitas@bristol.ac.uk)

Abstract

Constraining the mechanisms that control organic matter (OM) reactivity and, thus, degradation, preservation and burial in marine sediments across spatial and temporal scales is key to understanding carbon cycling in the past, present, and future. However, we still lack a quantitative understanding of what controls OM reactivity in marine sediments and, as a result, how to constrain it in global models. To fill this gap, we quantify apparent OM reactivity (i.e., model-derived estimates) by extracting reactive continuum model parameters (a and v) from observed benthic organic carbon and sulfate dynamics across 14 contrasting depositional settings distributed over five distinct benthic provinces. Our analysis shows that the large-scale range in apparent OM reactivity is largely driven by the wide variability in parameter a ($10^{-3} < a < 10^{7}$) with a high frequency of values in the range $10^{0} < a < 10^{4}$ years. In contrast, inversely determined v-values fall within a narrow range ($0.1 < v < 0.2$). Results also show that the variability in parameter a and, thus, in apparent OM reactivity is a function of the whole depositional environment, rather than the traditionally proposed, single environmental controls (e.g., water depth, sedimentation rate, OM fluxes). Thus, we caution against the simplifying use of a single environmental predictor for apparent OM reactivity beyond a specific local environmental context. In addition, diagenetic model results also indicate that, while

https://doi.org/10.5194/bg-2020-435
Preprint. Discussion started: 6 January 2021

Biogeosciences Discussions

OM fluxes exert a dominant control on depth-integrated OM degradation rates across most depositional environments, apparent OM reactivity becomes a dominant control in depositional environments that receive exceptionally reactive OM. Model results also show that apparent OM reactivity largely controls the relative significance of OM degradation pathways, and thus the redox zonation of the sediment, as well as depth of the sulfate-methane transition zone and rates of anaerobic oxidation of methane. Consequently, apparent OM reactivity also determines uptake and consumption of benthic terminal electron acceptors and nutrient recycling fluxes across a wide range of different depositional environments. In summary, our large-scale assessment not only further support the notion of apparent OM reactivity as a dynamic ecosystem property and highlights its crucial role for benthic biogeochemical cycling and exchange, but it also provides the first quantitative constraint on the most plausible range of reactivity parameters a and v. It thus represents an important advance for model parameterization as it largely alleviates the difficulty of determining OM reactivity in such models by constraining it to only one variable, i.e. the parameter a.

Key words: Reaction-Transport Model; seafloor; diagenesis; degradation rates, anaerobic oxidation of methane; sediment-water interface fluxes.

1 Introduction

Organic matter (OM) buried in marine sediments represents the largest reactive reservoir of reduced carbon on Earth (e.g., Hedges, 1992). The majority of OM that reaches modern global ocean seafloors originates from contemporary primary productivity (PP) in terrestrial (global net primary productivity, NPP, = ~59 Pg C y^{-1}) or marine environments (global NPP = ~49 Pg C y^{-1}). In addition, it also comprises OM derived from ancient PP, which is delivered through rock weathering, soil erosion, and thawing permafrost, as well as chemoautotrophy, and secondary production by microbes and animals (e.g., Hedges et al., 1997; Hedges and Oades, 1997). Since OM production slightly exceeds degradation, a small fraction of the photosynthetically produced organic carbon escapes heterotrophic degradation and is buried in sediments (Berner, 2003). This small imbalance between OM production and degradation connects the short- and long-term carbon cycles, controls the long-term evolution of atmospheric CO_2 and has enabled the accumulation of oxygen in the atmosphere (Berner, 2003; Hedges, 1992). Yet, compilations of field data reveal that OM degradation, and preservation rates vary significantly in space (Arndt et al., 2013; Burdige, 2006; Emerson and Hedges, 1988; Middelburg, 2019) and time (Berner, 2003). Significant progress has been made over the past decades in identifying the potential environmental controls of this spatio-temporal variability (Arndt et al., 2013; Bogus et al., 2012; LaRowe et al., 2020b; Zonneveld et al., 2010). It is becoming increasingly clear that the susceptibility of OM to heterotrophic degradation is not an inherent characteristic of the OM itself, but depends on its environmental context (e.g., Kayler et al., 2019; LaRowe et al., 2020b; Mayer, 1995; Zonneveld et al., 2010). In fact, OM reactivity is determined by the dynamic interplay of a plethora of different factors that include, but are not limited to OM sources and composition (Burdige, 2005; Hedges et al., 1997; Meyers, 1997); oxygen exposure time during settling and burial

https://doi.org/10.5194/bg-2020-435
Preprint. Discussion started: 6 January 2021

(Hartnett et al., 1998; Hoefs et al., 2002; Huguet et al., 2008; Sinninghe Damsté et al., 2002; Sun and Wakeham, 1994; Wakeham et al., 1997); terminal electron acceptor (TEA) availability (Aller, 1994; Aller and Aller, 1998); microbial activity (LaRowe et al., 2020b); sediment biological mixing (Aller, 1980, 1994; Aller and Aller, 1998; Boudreau, 1994; Grossi et al., 2003; Middelburg, 2018); OM ageing and transport history (Bianchi et al., 2018; Cathalot et al., 2010; Griffith et al., 2010; Mollenhauer et al., 2003, 2007; Ohkouchi et al., 2002); mineral protection through OM–sediment association (Bianchi et al., 2018; Hemingway et al., 2019; Keil and Cowie, 1999; Mayer, 1994a, 1994b); adsorption onto reactive iron minerals (e.g. Faust et al., 2020; Ma et al., 2018; Salvadó et al., 2015; Shields et al., 2016; Wang et al., 2019); or hydrogen sulfide exposure time (i.e., sulfurization) (Sinninghe Damsté et al., 1988, 1998). However, the relative significance of each of these factors remains poorly quantified. As a consequence, we currently lack a general framework that allows quantifying the reactivity of OM in a given environmental context. This knowledge gap seriously compromises our ability to constrain OM reactivity in both space and time (Arndt et al., 2013; Lessin et al., 2018), quantifying both pathways and rates of biogeochemical processes over different temporal and spatial scales (Hülse et al., 2018) and, thus, ultimately predicting the impact and feedbacks of past, present, and future climate change feedbacks on global biogeochemical cycles and climate.

Traditionally, apparent (i.e., estimated representation of) OM reactivity has been determined through laboratory-based incubation experiments in shallow (few centimetres deep) and mixed sediments (e.g., Dai et al., 2009; Grossi et al., 2003; Westrich and Berner, 1984) or integrated model-data approaches in deeply buried sediments (hundreds of centimetres to meters deep and hundreds to thousands and million years old) (e.g. Boudreau and Ruddick, 1991; Middelburg, 1989; Wehrmann et al., 2013), using Reaction-Transport Models (RTM). Especially the latter are powerful tools since they allow the extraction of quantitative measures of OM reactivity from comprehensive multi-species porewater datasets integrated over greater sediment depths/ages. RTMs can be broadly subdivided into two classes regarding OM conceptualisation: discrete models and continuum models (e.g., Arndt et al., 2013). Discrete or G-type models (Berner, 1980), and particularly multi-G models (Jørgensen, 1978; Soetaert et al., 1996; Westrich and Berner, 1984) compartmentalise OM into discrete pools each having distinct reactivity. Although mathematically simple, multi-G models require the definition of both the size and reactivity of its discrete OM pools. Observational data generally allows unequivocal identification of a maximum number of three distinct compound classes (Jørgensen, 1978; Middelburg, 1989). Continuum models (Boudreau and Ruddick, 1991; Middelburg, 1989) on the other hand are mathematically more complex models, which assume a continuous distribution of OM compounds over the entire reactivity spectrum, thus avoiding the partitioning of OM into a discrete compound classes. Unlike Multi-G models that converge towards a constant reactivity once more reactive compound classes are depleted at depth, continuum models account for the widely observed continuous decrease in OM reactivity with sediment depth. Consequently, the application of multi-G models is limited to shallow, contemporary sediments (Ait Ballagh et al., 2020; Dale et al., 2008a, 2008b, 2015; Luff et al., 2000; Paraska et al., 2014; Soetaert et al., 1996; Stolpovsky et al., 2018), whereas continuum models are successfully employed in both shallow, contemporary environments, as well as deeply buried, old sediments (Arndt et al., 2009; Boudreau and Ruddick, 1991; Bradley et al., 2020; Contreras et al., 2013; Henkel et al., 2012; Jørgensen et al., 2019a; LaRowe et al.,

https://doi.org/10.5194/bg-2020-435
Preprint. Discussion started: 6 January 2021

2020a; Mogollón et al., 2012, 2016; Wehrmann et al., 2013; Ye et al., 2016). However, due to our limited quantitative understanding of the environmental controls on OM reactivity, the application of both model types to data-poor settings is still complicated by the difficulty in constraining model parameters, inducing important uncertainties at the global scale as well as past and future applications.

In a first attempt to address this knowledge gap, Arndt et al. (2013) compiled a comprehensive global dataset of previously published, model-derived apparent OM reactivities across a wide range of depositional environments. Their analysis revealed that reactivity is largely variable within each sedimentary setting with no clear global trends. Nevertheless, broad regional reactivity trends were highlighted. For instance, the highly productive upwelling region of the Arabian Sea is characterized by the burial of highly reactive OM. Monsoon-induced high PP rates and an associated pronounced oxygen minimum zone (OMZ) promote an efficient export and burial of fresh, reactive OM (Cowie, 2005; Koho et al., 2013; Luff et al., 2000; Rixen et al., 2019; Vandewiele et al., 2009). In coastal settings and continental margins, a high variability in OM reactivity is attributed to variable inputs of terrestrial and marine OM with complex degrees of alteration prior to burial (Hedges et al., 1997; Oni et al., 2015b). In open ocean sediments, a large range in the reactivity spectra arises from several processes operating simultaneously at great water depths; e.g., efficient degradation during settling (Emerson and Hedges, 1988; Sun and Wakeham, 1994; Wakeham et al., 1997), extensive exposure time to oxygen (Hartnett et al., 1998; Mewes et al., 2014, 2016; Mogollón et al., 2016; Volz et al., 2018), and ageing (Griffith et al., 2010). The global compilation of OM reactivity (Arndt et al., 2013) also revealed a lack of significant global correlation between OM reactivity and single characteristics of the depositional environment (water depth, sedimentation rate, OM fluxes), thus confirming cautious statements regarding the global validity of previously published relationships (Boudreau, 1997; Müller and Suess, 1979; Tromp et al., 1995) and emphasising the role of a complex interplay of environmental controls on reactivity (e.g., Kayler et al., 2019; LaRowe et al., 2020b; Mayer, 1995; Zonneveld et al., 2010).

Crucially, the analysis by Arndt et al. (2013) revealed that a lack of comparative studies was a roadblock towards developing a robust global scale framework for OM reactivity. The large variability in model formulation and approaches adopted by different studies limits the comparability and transferability of results (Arndt et al., 2013), which hampers our ability to develop a systematic understanding of processes controlling OM reactivity on a global scale and OM cycling in the past, present, and future (Hülse et al., 2018). Therefore, we here use a consistent, integrated model-data approach to inversely determine the parameters that control apparent OM reactivity in the Reactive Continuum Model (RCM), a and v (Boudreau and Ruddick, 1991) from contemporary sediment depth profiles (Sect. 3) at 14 different sites from five different depositional environments (Sect. 2). Briefly, those parameters, alongside burial age, determine the depth-evolution of apparent OM reactivity; and consequently, OM degradation dynamics (see Sect. 3.2 for details). The large-scale variability in inversely determined parameters a and v is then assessed and first order constraints on model parametrization are provided. Additionally, following the approach of Arndt et al. (2013), we compile a and v values derived from previously published data-model approaches

https://doi.org/10.5194/bg-2020-435
Preprint. Discussion started: 6 January 2021

(Arndt et al., 2009; Boudreau and Ruddick, 1991; Contreras et al., 2013; Henkel et al., 2012; Mewes et al., 2016; Mogollón et al., 2012, 2016; Wehrmann et al., 2013; Ye et al., 2016). Inversely determined parameters are compared to previously published values and the extended dataset is then used to explore the links between OM reactivity and master characteristics of depositional environments. Furthermore, we quantify key processes associated with OM transformation within sediments to assess the role of OM reactivity on benthic biogeochemical cycling. From our model simulations, we estimate OM degradation rates and relative contributions of metabolic pathways, anaerobic oxidation of methane coupled to sulfate reduction (AOM) rates, as well as dissolved TEA and nutrient fluxes across the SWI. With this comprehensive and global-scale approach, we aim to explore the links between OM reactivity and characteristics of depositional environments, and to understand the controls of reactivity on OM transformation processes.

2 Study sites

Our data-model study covers a wide range of depositional environments, from coastal to shelf and slope settings characterized by widely different environmental conditions (Fig. 1, Table 1). It comprises the following benthic provinces (Seiter et al., 2004): Northern European margin (EUR1); NW Mediterranean margin off Rhone delta (EUR2); Western Arabian Sea (WARAB); Bering Sea (NWPAC); and SW Atlantic off La Plata river (RIOPLATA). Most of those regions are characterised by predominantly temperate climate regimes, except for the Arabian Sea region (Arid) and the Bering Sea area (Snow/Polar) (Chen and Chen, 2013). OM characteristics also cover a broad spectrum, ranging from organic rich (TOC > 2 wt%) to lean (TOC < 1 wt%) sediments (Premuzic et al., 1982; Seiter et al., 2004), and from predominantly terrestrial (coast), mixed terrestrial and marine (coast/shelf) to predominantly marine (shelf/slope) OM (Hedges et al., 1997; Meyers, 1997). The pelagic ecosystem structure reflects local and regional characteristics. Overall, as a common characteristic they display the occurrence of spring/summer phytoplankton blooms, which are triggered by various mechanisms (Table 1). This is also reflected by the composition of the phytoplankton community, and thus OM production at the photic zone and vertical transport efficiency to sediments (e.g., Bach et al., 2019). This wide spectrum of depositional environments (Table 1) offers a unique opportunity to quantify OM reactivity and explore its multidisciplinary links with environmental drivers.

3 Methods

Here, we adopt an integrated model-data approach to inversely determine OM reactivity parameters a and v from contemporary TOC and SO_4^{2-} profiles measured at 14 sites across the five different depositional environments described in Sect. 2. The following sections provide an overview of the observational data (Sect. 3.1), a detailed description of the applied RTM (Sect. 3.2), an overview of the inverse model approach used to extract RCM parameters from the observed depth profiles (Sect. 3.2.3), as well as a summary of the analysed model output (section 3.2.4).

https://doi.org/10.5194/bg-2020-435
Preprint. Discussion started: 6 January 2021

3.1 Observational Data

We benefit from previously published datasets to develop our global-scale OM reactivity assessments. TOC and porewater SO_4^{2-} depth-profiles, as well as site-specific physical characteristics and supporting data are available for all sites and were compiled from the PANGAEA database (www.pangaea.de) (except from Rhone delta and Severn estuary datasets), as well as corresponding published literature (see below). Specific details about sampling strategies and analytical methods can be found in the respective publications. The dataset for the Severn estuary (Table 1; row A) are from Thomas (2014). Rhone delta data (Table 1; rows B and C) are from the DICASE project (Rassmann et al., 2016). Data for the Northern European margin sites Aarhus Bay, Arkona Basin, and the Skagerrak transect (Table 1; rows D, E, G, H, and I) are part of the European funded project METROL (Aquilina et al., 2010; Dale et al., 2008a, 2008b; Knab et al., 2008; Mogollón et al., 2012). Data from the Helgoland Mud Area, North Sea (Table 1; row F) (Henkel and Kulkarni, 2015), the Arabian Sea transect (Table 1; rows J, K, and L) (Bohrmann and cruise participants, 2010a, 2010b, 2010c), Bering Sea (Table 1; row M) (Gersonde, 2009), and Argentine Basin (Table 1; row N) (Henkel et al., 2011) are presented on PANGAEA database (see above). We use those site-specific datasets to inform our data-model analysis and to constrain OM reactivity and related benthic processes (Sect. 3.2.2 and 3.2.3).

3.2 Model description

The Biogeochemical Reaction Network Simulator (BRNS) (Aguilera et al., 2005; Regnier et al., 2002) is an adaptive simulation environment that has been successfully employed to reproduce and quantify diagenetic processes in marine sediments across a wide range of depositional environments and timescales (Dale et al., 2008a; Thullner et al., 2009; Wehrmann et al., 2013). The BRNS is suitable for large, mixed kinetic-equilibrium reaction networks (Dale et al., 2009; Jourabchi, 2005; Thullner et al., 2009). Here, we design a BRNS set-up that explicitly resolves the fluxes and transformations of OM (CH_2O), the most pertinent TEAs (oxygen – O_2; nitrate – NO_3^-; and sulfate – SO_4^{2-}) and reduced species (methane – CH_4; sulfide - HS^-; and ammonium – NH_4^+). Due to the limited availability of data to constrain manganese oxide (MnO_2) and iron hydroxide ($Fe(OH)_3$) depositional fluxes, the model does not account for metal oxides reduction pathways. At certain depositional settings (e.g., Skagerrak), metal oxides can be relatively important TEAs (e.g., Canfield et al., 1993; Rysgaard et al., 2001), particularly in continental margins that receive considerable inputs of iron (Beckler et al., 2016). Nevertheless, a previously published global assessment of the importance of metabolic pathways in marine sediments has found their contributions to the overall heterotrophic OM degradation to be negligible at a global scale (Thullner et al., 2009). For each of the species i involved in heterotrophic OM degradation, the BRNS simulates changes in both solid phase and porewater concentrations C_i as result of transport processes (advection, molecular diffusion, bioirrigation and bioturbation), as well production/consumption due to reactions (Aguilera et al., 2005; Thullner et al., 2009; Wehrmann et al., 2013). In the following

https://doi.org/10.5194/bg-2020-435
Preprint. Discussion started: 6 January 2021

sections we provide a detailed description of the model approach, including parameters values (Table 2), boundary conditions (Table 3), rates (see Table S1 for stoichiometric equations) and fluxes calculations.

3.2.1 Model formulation

The concentration depth profiles of solid and dissolved species in marine sediments are calculated according to the vertically-resolved mass conservation equation of solid and dissolved species C_i in porous media (Berner, 1980; Boudreau, 1997):

$$\frac{\partial \sigma C_i}{\partial t} = \frac{\partial}{\partial z}\left(D_{bio}\sigma \frac{\partial C_i}{\partial z} + D_i \sigma \frac{\partial C_i}{\partial z}\right) - \frac{\partial \sigma \omega C_i}{\partial z} + a_i \sigma (C_i(0) - C_i) + \sum_j s_i^j R^j \quad (1)$$

where C_i is the concentration of specie i, t denotes time, and z is the sediment depth. For solid species, the porosity term is given by $\sigma = (1 - \varphi)$, whereas for dissolved species porosity assumes $\sigma = \varphi$. The effective molecular diffusion coefficient of dissolved species i is given by D_i ($D_i = 0$ for solid species), D_{bio} represents the bioturbation coefficient, ω the sedimentation rate, and a_i denotes the bioirrigation coefficient ($a_i = 0$ for solid species). The sum of consumption/production process rates is given by $\sum_j s_i^j R^j$, where the stoichiometric coefficient of specie i is given by s_i^j for the kinetically controlled reaction j, with rate R^j.

3.2.1.1 Transport processes and parameters

The RTM accounts for sediment accumulation and compaction, molecular diffusion, bioturbation, and bioirrigation (see Eq. 1). Sediment porosity is assumed to decrease exponentially with depth due to sediment compaction:

$$\varphi_z = \varphi_\infty + (\varphi_0 - \varphi_\infty) exp(-\beta z) \quad (2)$$

where β is the porosity attenuation coefficient, φ_z is the porosity at depth and φ_∞ is the porosity at greater depth. Consequently, the burial velocity is corrected for the effect of compaction assuming steady state compaction (e.g. Berner, 1980):

$$\omega_z = \omega_0 (1 - \varphi_0)/(1 - \varphi_z) \quad (3).$$

The diffusive fluxes are commonly quantified by means of Fick's first law of diffusion, which depends on the molecular diffusive coefficient D_i (i = dissolved species) and is corrected for sediment tortuosity. D_i is dependent on the charge and size of the diffusing species, as well as temperature and viscosity of the medium (Boudreau, 1997; Burdige, 2006). Here, D_i are corrected for temperature, salinity, and tortuosity. The model also accounts for the effect of sediment reworking by infaunal

https://doi.org/10.5194/bg-2020-435
Preprint. Discussion started: 6 January 2021

organisms in the bioturbated upper sediment layer ($z < z_{bio}$). The process is generally described by a dispersive term with constant bioturbation diffusion coefficient D_{bio} (Boudreau, 1986). Bioirrigation, i.e. the mixing by benthic macrofaunal organisms that build burrows or tubes in the sediment for feeding is described as a nonlocal transport process with a nonlocal bioirrigation coefficient a_i, which describes the exchange rates between SWI and porewater at depth in bioirrigated zone of sediments (Aller, 1994; Aller and Aller, 1998; Burdige, 2006).

Implemented transport parameters can be subdivided into two classes: (i) global model parameters (Table 2), which are universal for all depositional environments, and thus assure model transferability across sites; and (ii) site-specific transport parameters (Table 3), which are constrained for each depositional environment investigated here, either by direct observations or derived from empirical relationships.

3.2.1.2 Reaction network

The reaction network implemented here encompasses the most pertinent primary and secondary redox reactions found in the upper layers of marine sediments. Its formulation and parametrization builds on a number of previous studies that investigate diagenetic dynamics across several depositional environments and scales (Aguilera et al., 2005; Thullner et al., 2009; Van Cappellen and Wang, 1996; Wang and Van Cappellen, 1996; Wehrmann et al., 2013). It explicitly accounts for the heterotrophic degradation of OM coupled to the consumption of oxygen (aerobic OM degradation), nitrate (denitrification), sulfate (organoclastic sulfate reduction), as well as methanogenesis. Additionally, it accounts for nitrification, sulfide re-oxidation by O_2 (in the absence of $Fe(OH)_3$, which would most likely be responsible for re-oxidation of sulfides; e.g., Findley et al. (2020)), anaerobic oxidation of methane coupled to sulfate reduction (AOM) and CH_4 reoxidation by O_2. Stoichiometric reactions and kinetic rate formulations for each of the primary and secondary redox reactions involved in OM heterotrophic degradation are summarized in the Supplements (Table S1 and Table S2).

OM degradation rates R_C are calculated assuming that the bulk OM is continuously distributed over a range of reactivities k, i.e. a reactive continuum model (RCM). OM is degraded according to first-order kinetics with respect to the electron donor, (i.e. particulate organic matter (POM) which is assumed to be $(CH_2O)_{106}(NH_3)_{16}(H_3PO_4)$). A recent study on the sensitivity of OM stoichiometry towards degradation dynamics (Arning et al., 2016) supports the use of CH_2O simplification for describing complex OM composition. As such, the overall rate of OM degradation R_C for a continuous distribution of organic compounds is given by the integral:

$$R_C = -\int_0^\infty k \cdot om(k,t)dk \quad (4)$$

https://doi.org/10.5194/bg-2020-435
Preprint. Discussion started: 6 January 2021

where $om(k,t)$ denotes the probability density function that determines the concentration of OM having a degradability between k and $k+dk$ at time t, with k being equivalent to the first-order degradation rate constant. At $t=0$, the initial OM distribution $om(k,0)$ can assume distinct mathematical formulations, however it cannot be constrained from observations. Here, a Gamma function is adopted (Aris, 1968; Boudreau and Ruddick, 1991; Ho and Aris, 1987). Assuming first-order degradation kinetics, the initial distribution ($t=0$) of OM is given by:

$$om(k,0) = \frac{POC(0)\cdot\alpha^{\nu}\cdot k^{\nu-1}\cdot e^{-\alpha\cdot k}}{\tau(\nu)} \quad (5)$$

where $POC(0)$ denotes the initial OM content, τ is the Gamma function, α is the average lifetime of the more reactive components of bulk OM, and ν represents the dimensionless scaling parameter of the distribution near $k=0$. The free, positive parameters α and ν delineate the shape of the initial distribution of OM compounds along the range of k, and thus the overall reactivity of bulk OM. As such, the RCM approach requires the definition of two parameters that will define the shape of the OM distribution over reactivity k.

Due to the rapid depletion of the most reactive compounds, the reactivity of the bulk material decreases during degradation and thus reflects the widely observed reactivity decrease with burial time/depth/age (Boudreau and Ruddick, 1991; Middelburg, 1989). In the RCM, OM compounds are continuously and dynamically distributed over a range of reactivities that captures the decrease in apparent reactivity with burial age/depth as the most reactive compounds are successively degraded. The interplay of α and ν drives the bulk OM reactivity depth profiles and consequently the yielded profiles from the reaction network implemented in the BRNS. The Gamma distribution captures the OM degradation dynamics in nature. As such, the evolution of OM concentration as a function of depth z ($POC(z)$) is given by:

$$POC(z) = POC(0)\cdot\left(\frac{\alpha}{\alpha+age(z)}\right)^{\nu} \quad (6)$$

where α and ν are the free RCM parameters (Arndt et al., 2013; Boudreau and Ruddick, 1991) and $age(z)$ denotes the age of the sediment layer at depth z. For non-bioturbated sediments the burial age ($z = z - z_{bio}$) can be calculated as a function of the burial velocity and is given by:

$$age(z) = age_0 + \frac{(1-\varphi)z+\beta^{-1}(\varphi_0-\varphi_\infty)(exp(-\beta z)-1)}{\omega(1-\varphi_0)} \quad (7)$$

where age_0 is the initial age at the bottom of the bioturbated zone, β is the porosity attenuation coefficient, φ_z is the porosity at depth and φ_∞ is the porosity at greater depth. However, within the bioturbated upper sediment layers, the age distribution

https://doi.org/10.5194/bg-2020-435
Preprint. Discussion started: 6 January 2021

of reactive species is controlled by both sedimentation, bioturbation, and the reactivity k of reactive species (Meile and Van Cappellen, 2005). Thus, we here apply a multi-G approximation for the RCM in the bioturbated sediments (Sect. 3.2.1.3).

The sequential utilisation of TEA is described by a combination of Michalis-Menten and inhibition terms. The rate of heterotrophic OM degradation is independent of the TEA concentration for TEA > K_j (j = TEA). However, for low TEA concentrations, the specific OM degradation pathway rate becomes limited by TEA availability, expressed as a first-order dependency of the rate with respect to the TEA (Table S2). TEAs are consumed sequentially following the decrease in *Gibbs free energy yield* of the respective metabolic pathway reactions. The resulting classic redox sequence is described by a sequence of inhibition terms f_j, where j denotes the TEA consumed by the respective metabolic pathway:

$$f_j = \left(1 - \sum_{n<j} f_n\right) \quad \text{if} \quad j > K_j \tag{8}$$

$$f_j = \left(1 - \sum_{n<j} f_n\right) \cdot \frac{j}{K_j} \quad \text{if} \quad j \leq K_j \tag{9}.$$

After all TEAs are depleted, OM degradation proceeds via methanogenesis. In addition to primary redox reactions, the reaction network also accounts for secondary redox reactions, i.e. re-oxidation of reduced species produced during primary redox reactions. Following the classical approach, the rates of secondary redox reactions are described by biomolecular rate laws with the rate constant k_i (Table 2 and Table S1) (Van Cappellen and Wang, 1996).

3.2.1.3 Multi-G approximation of RCM in the bioturbated layer

Within the bioturbated layer ($z < z_{bio}$), the RCM is approximated by a multi-G model (200 fractions) to circumvent the difficulty of quantifying OM ages within bioturbated sediments (Dale et al., 2015; Meile and Van Cappellen, 2005). The multi-G model approach divides the bulk OM into multiple discrete compound classes i, each degrading according to first-order kinetics with a degradation rate constant k_i (Jørgensen, 1978). It thus accounts for the heterogeneity of bulk OM by assigning different reactivities to each pool of organic matter (G_i) (Arndt et al., 2013). The RCM is approximated by dividing the initial, continuous distribution of OM compounds over the reactivity spectrum (Eq. 4) into discrete compound classes. The fraction of total OM F_i in compound class i can be directly calculated by integrating the initial probability density function (Eq. 4), which determines the concentration of OM having a degradability between k_j and $k_j + dk_j$ at time zero with:

$$k_i = \frac{k_{j+1}}{2dk_j} \tag{10}.$$

https://doi.org/10.5194/bg-2020-435
Preprint. Discussion started: 6 January 2021

In bioturbated sediments, the RCM is then approximated by dividing the defined reactivity range $k = [10^{-15},\ 10^{-\log(\alpha)+2}]$ into 200 equally spaced reactivity pools k_j. The initial fraction F_i of total POC in compound class i defined by the reactivity bin k_{j-1} and k_j in the 200-G model can be calculated as:

$$F_i = F(k_j, 0) - F(k_{j-1}, 0) \quad (11).$$

The least and the most reactive fractions F_1 and F_{200} with reactivity $k_1 = 10^{-15}$ and $k_{200} = 10^{-\log(\alpha)+2}$ y^{-1}, respectively, are calculated based on the upper incomplete Gamma function:

$$F_1 = \int_{k_1}^{\infty} f(k_1, 0)dk = \frac{\tau(v, ak_1)}{\tau(v)} \quad (12)$$

$$F_{200} = \int_{k_{200}}^{\infty} f(k_{200}, 0)dk = \frac{\tau(v, ak_{200})}{\tau(v)} \quad (13).$$

Once F_i and k_i are determined, the steady-state solution of the diffusion-advection-reaction equation (Boudreau, 1997) for OM in the bioturbated zone is then given by the general analytical solution:

$$POC(z) = \sum_{i=1}^{200} Ai \cdot \exp(ai \cdot z) + Bi \cdot \exp(bi \cdot z) \quad (14)$$

with:

$$ai = \frac{\omega - \sqrt{\omega^2 + 4 \cdot D_{bio} \cdot k_i}}{2 \cdot D_{bio}} \quad (15)$$

and

$$bi = \frac{\omega + \sqrt{\omega^2 + 4 \cdot D_{bio} \cdot k_i}}{2 \cdot D_{bio}} \quad (16).$$

A and B denote integration constants that can be determined by defining appropriate boundary conditions (Boudreau, 1997) for OM at the upper and lower boundaries. Below the bioturbated zone, the depth evolution of POC is determined by the RCM formulation (Eq. 6).

https://doi.org/10.5194/bg-2020-435
Preprint. Discussion started: 6 January 2021


Biogeosciences Discussions

3.2.1.4 Additional model parameters

The bioirrigation rate a_i was calculated from the bioirrigation coefficient at sediment surface a_0 and the bioirrigation attenuation depth length x_{irri} (Thullner et al., 2009; Wehrmann et al., 2013):

$$a_i = a_0 \cdot exp(-x/x_{irri}) \quad (17).$$

The effective molecular diffusion coefficients D_i for each of the species i (Table 2) are derived from Van Cappelen and Wang (1996). D_i values are corrected for temperature (T), salinity (S) and tortuosity (φ^2). For solid species $D_i = 0$, whereas for dissolved species the corrected D_i^* is given by Boudreau (1997):

$$D_i^* = \frac{D_i(T,S)}{1-ln(\varphi^2)} \quad (18).$$

Sediment porosity φ_0, φ_∞, β, sedimentation rate ω, and temperature T were either measured at site or derived from literature when actual measurements were not available. Salinity S was defined as 35 at all sites. Bioturbation depth z_{bio} was fixed at 10 cm for most bioturbated sediments (Table 3), based on a compilation of mixed layer depths (Boudreau, 1994, 1998). At anoxic depositional environments (i.e., where O_2 concentrations are zero), z_{bio} was set to zero (Table 3). Similarly, the bioturbation diffusion coefficient D_{bio} was set to zero at anoxic environments. For bioturbated sites, D_{bio} was constrained based on an empirically derived relationship proposed by Middelburg et al. (1997):

$$D_{bio} = 5.2 \cdot 10^{(0.7624-0.0003972 \cdot h)} \quad (19)$$

where h denotes the water depth. For the Rhone delta, D_{bio} values were derived from Pastor et al. (2011). D_{bio} was kept constant within the bioturbated zone ($z < z_{bio}$) then set to zero below z_{bio}.

The reaction parameters (except for the RCM parameters α and v) implemented in the BRNS are universal for all depositional environments (Table 2). This approach ensures that model set-ups are consistent and model-derived RCM parameters are independent of model formulation and fully comparable across depositional settings. The half-saturation concentrations K_i of the respective Michaelis-Menten terms were adopted from Van Cappellen and Wang (1996). Secondary redox reaction constants for each explicitly resolved reaction are based on a compilation of published values (Dale et al., 2011). The RCM parameters α and v reflect the site-specific OM reactivity and are free parameters that are determined by inverse modelling (Sect. 3.3).

https://doi.org/10.5194/bg-2020-435
Preprint. Discussion started: 6 January 2021

3.2.1.5 Boundary conditions

Boundary conditions place the BRNS in the environmental context of each of the study sites (Table 3). The boundary conditions are constrained based on either site-specific measurements or alternatively on published data if direct observations were not available. Here, we assume a fixed boundary concentration (POC_0) of OM at the sediment water interface. Concentrations of O_2 are based on measurements in Skagerrak (Canfield et al., 1993) and Rhone delta (Rassmann et al., 2016) sediments. Similarly, concentrations of NO_3^- are based on measurements in Skagerrak sediments (Canfield et al., 1993). Because of the lack of site specific information, these O_2 and NO_3^- are adopted at all oxic sites (where SO_4^{2-} > 28 mM) since they are representative for coastal and shallow slope sites and their exact value exerts no influence on deep SO_4^{2-} and CH_4 concentrations. For anoxic sites (where SO_4^{2-} < 28 mM), O_2 and NO_3^- bottom water concentrations are set to zero. SO_4^{2-} concentrations were constrained based on measurements for each of the simulated sites. Concentrations of CH_4 and HS^- were set to zero at SWI, as those species are rapidly oxidised in the overlying bottom water. A no flux $\left(\frac{\partial C}{\partial z} = 0\right)$ condition was implemented for all species at the lower boundary, assuming that biogeochemical dynamics in underlying sediments exert no influence on diagenetic processes in the model domain.

3.2.2 Model solution

Transport and reaction equations were solved sequentially. Firstly, the diffusion term was discretized at each time-step of the numerical integration using the semi-implicit Crank-Nicholson scheme. This was followed by the calculation of the advective transport, using a 3rd order accurate total variation diminishing algorithm with flux limiters (Regnier et al., 1998). The reaction network was subsequently solved. The mass-conservation equation (Eq. 1) was discretized on an uneven grid (Boudreau, 1997):

$$z(n) = \frac{L\left(\left(\xi_n^2+\xi_c^2\right)^{0.5}-\xi_c\right)}{\left(L^2+\xi_c^2\right)^{0.5}-\xi_c} \quad (20)$$

where $z(n)$ is the depth of the n^{th} grid point, L denotes the length of the model domain, ξ_n is a point in a hypothetical grid, and ξ_c is depth relative to which $z(n)$ is quadratically distributed for $\xi_n \ll \xi_n$ and linearly distributed for $\xi_n \gg \xi_n$. L and ξ_n were chosen so that the grid size, Δz, increases downcore from SWI to a maximum of L. The size of model domain L was fixed at 1,000 cm for all sites, except for the Bering Sea, in which the model domain is extended to 1,500 cm, due to the low sedimentation rate assumed for this site (Table 2). This choice is based on initial tests and ensures that the model domain

https://doi.org/10.5194/bg-2020-435
Preprint. Discussion started: 6 January 2021

covers the diagenetically most active zone, thus reducing the influence of biogeochemical dynamics in underlying sediments on biogeochemical dynamics within the model domain. BRNS was run until steady state ($\Delta t < 0.01$) was reached:

$$run\ time = 2 \cdot \frac{z}{\omega} \quad (21).$$

The assumption of steady-state condition for estuarine sites may be impacted by the high dynamic nature of such settings. At the Severn estuary a strong tidal dynamics results in continuous cycles of sediment resuspension (Manning et al., 2010). The Rhone delta experiences strong pulses of fresh water and sediments associated to flood events, as well as variable sedimentation rates (Antonelli et al., 2008; Cathalot et al., 2010; Zebracki et al., 2015). Despite that (and somewhat surprisingly), previous investigations at the Rhone delta found similar biogeochemical trends on an interannual basis, i.e. data collected along the years in this system are consistent (Dumoulin et al., 2018; Pastor et al., 2011; Rassmann et al., 2016, 2020). As such, it is likely that the majority of sediment load and OM are delivered during late fall and early winter flood events, and the diagenetic system close to the river mouth reaches a mature state during early spring when the typical porewater and benthic-pelagic fluxes have established. A surprisingly similar steady benthic cycling has been observed along a sea–sea-ice gradient at the Barents Sea shelf, which is a very seasonally dominated environment (Freitas et al., 2020). Thus, for the purpose of our investigations, we assume that on longer time/depth scales those sediments reach steady state and the limitations imposed should be minimal.

3.2.3 Inverse modelling

Here, we apply the BRNS to determine RCM parameters (α and v) from present-day downcore observations by inverse modelling of observed depth profiles (e.g., Arndt et al., 2009; Wehrmann et al., 2013). The first efforts to quantify α and v parameter values, and thus reactivity, on the basis of observations solely focused on downcore TOC profiles (Boudreau and Ruddick, 1991). While this approach has provided useful insights, it is nevertheless compromised by several factors. First, it is generally difficult to quantify OM contents at the sediment-water interface (SWI) due to the common loss of the upper few centimetres during sampling with gravity or piston corers. In addition, a steady-state OM deposition over the entire time span of sediment deposition is unlikely, especially in slope and coastal settings. Finally, multiple α and v pairs could potentially fit a given TOC depth profile (Meister et al., 2013). Parameter estimates based on TOC profiles alone are thus associated with a generally unknown degree of uncertainty.

Adding further constraints increases the robustness of predictions. OM heterotrophic degradation is the driver behind biogeochemical dynamics in marine sediments, and downcore profiles of TEAs (e.g., SO_4^{2-}) (e.g., Bowles et al., 2014; Jørgensen et al., 2019b) or reduced products of OM degradation (such as CH_4 and NH_4^+) provide further constraints. To

https://doi.org/10.5194/bg-2020-435
Preprint. Discussion started: 6 January 2021

determine a minimum set of observational data that is widely available and comparably easy to measure, we tested the suitability of different artificial porewater data sets for the inverse determination of apparent OM reactivity. Using an artificially generated dataset (see Supplements, Table S3), we ran the BRNS in the same fashion as we did for the site-specific data-model approach (see below). Our sensitivity analysis confirms that when TOC is considered as a single constraint, multiple pairs of a and v produce equivalent TOC depth-profiles (Supplements, Fig. S1), as previously suggested (Meister et al., 2013). Model results show that by adding SO_4^{2-} depth profiles as an additional constraint (Supplements, Fig. S2), the determination of a and v becomes more robust (Supplements, Fig. S3). CH_4 profiles were used as an additional constraint when the data were available, although measured *ex situ* CH_4 profiles are often not reliable due to sampling and measurement uncertainties in deeper sediment layers where concentrations exceed mM (Dale et al., 2008a; Hensen et al., 2003; Hilligsøe et al., 2018). The dynamics of SO_4^{2-} and CH_4 are solely controlled by OM degradation and AOM (e.g., Bowles et al., 2014; Egger et al., 2018; Regnier et al., 2011), although their distributions can be also affected by bioirrigation in particularly shallow sulfate-methane transition zones (SMTZs) (e.g., Dale et al., 2019). In anoxic settings and deeply buried sediments, SO_4^{2-} is the dominant TEA and CH_4 is the most common reduced species (Jørgensen et al., 2019a, 2019b). Thus, a combination of TOC, SO_4^{2-}, and CH_4 (if available to verify the depths of the SMTZ) depth profiles incorporates the information contained in the observed benthic sulfur and carbon dynamics and is sufficient to extract apparent OM reactivity and its evolution from the sediment-water interface down to the SMTZ. Thus, here we perform a site-specific data-model fit based on TOC and SO_4^{2-} (and CH_4) depth profiles. The RCM parameters were inversely determined by running the model for each site over the entire range of previously published α ($a = 10^{-3} – 10^{7}$ years) and v ($v = 10^{-2} – 10^{0}$) values. First, the model was run over a coarsely resolved ensemble of α and v combinations to explore the order of magnitude in which the RCM parameters fall. Once the order of magnitude was established, a new model ensemble was run over a finely resolved grid of α and v pairs falling in the previously defined range.

3.2.4 Quantification of organic matter reactivity and associated benthic processes

The apparent reactivity of bulk OM k for each site is calculated based on the RCM reactivity parameters a and v (Boudreau and Ruddick, 1991) that yield the best data-model fit and is given by:

$$k(z) = \frac{v}{(\alpha + age(z))} \quad (22).$$

The apparent reactivity of bulk OM at the sediment water interface ($z = 0$) is thus given by:

$$k(0) = \frac{v}{a} \quad (23).$$

https://doi.org/10.5194/bg-2020-435
Preprint. Discussion started: 6 January 2021

The BRNS simulates downcore concentration profiles for each species i that is explicitly resolved in the reaction network, as well as reaction rates r_n. From those reaction rates, the total rate of organic carbon oxidation, i.e. the depth integral of R_C for each primary redox reaction n can be calculated by integrating the rate over the entire model domain L (e.g., Thullner et al., 2009):

$$\sum R_C = \sum_n \int_0^L r_n dx \quad (24).$$

The OM fluxes (F_{OM}) at the SWI are calculated based on the sum of $\sum R_C$ and burial fluxes (e.g. Burdige, 2006):

$$F_{OM} = \sum R_C + F_{burial} \quad (25)$$

$$F_{burial} = (1 - \varphi_z) \cdot \omega_z \cdot POC_z \quad (26).$$

Additionally, the fluxes of species i at the SWI, i.e. the benthic-pelagic fluxes, are calculated from the model-derived depth profiles of species i according to:

$$J_i = J_{i,Advection} + J_{i,Diffusion} + J_{i,Bioturbation} + J_{i,Bioirrigation} \quad (27).$$

In such calculations, positive J_i values indicate upward fluxes from the sediment, whereas negative values represent downward fluxes into the sediment.

4 Results and discussion

The integrated data-model analysis yielded a comprehensive picture of OM reactivity parameters (a, v, and $k(z)$), as well as OM degradation dynamics and benthic-pelagic coupling for our large-scale compilation of depositional environments (Table 4). Because model parameters implicitly account for all the processes that are not explicitly described in the model, this variability provides important insights into the environmental controls on OM reactivity. In the following sections, we explore the inverse modelling results in the context of their depositional environment, (e.g. water depth, sedimentation rates, and OM fluxes, bottom water and sediment redox conditions, OM quality, and mineral protection), explore emerging patterns and provide important, first order constraints on model parameterization.

https://doi.org/10.5194/bg-2020-435
Preprint. Discussion started: 6 January 2021

4.1 Constraining apparent OM reactivity

4.1.1 Inverse Modelling

We inversely determined the set of RCM parameters a and v that produces the best model fit to the observed TOC (Fig. 2) and SO_4^{2-} (Fig. 3) depth-profiles. Overall, TOC profiles display a satisfying fit between model and observations. However, the quality of fit is often compromised by a lack of observations/data at the SWI due to core loss during sediment sampling by gravity and piston corers, as well as a poor downcore sampling resolution. Therefore, determining the reactivity parameters based solely on TOC observations, an approach adopted in the past (Boudreau and Ruddick, 1991), would not be feasible for those sites and adding additional constraints relieves such limitation. The SO_4^{2-} depth-profiles (Fig. 3) display a good agreement between present-day observations and model simulations, except for the Arabian Sea site below the OMZ (Fig. 3l) and the Bering Sea (Fig. 3m). At the Bering Sea, the data-model discrepancy is likely associated to kinks in both TOC (Fig. 2m) and SO_4^{2-} (Fig. 3m) profiles. They likely represent changes in the depositional regime (non-steady state) over the studied timescale (e.g., Hensen et al., 2003) that are not captured by the model. The mismatch in the Arabian Sea at the site below the OMZ (Fig. 3l) could originate from SO_4^{2-} recycling through H_2S oxidation by MnO_2 and $Fe(OH)_3$ (e.g., Rassmann et al., 2020; Schulz et al., 1994), however we are unable to further explore this hypothesis due to a lack of metal oxide data to constrain those biogeochemical reactions.

4.1.2 Apparent OM reactivity parameters v and a

The inversely determined OM reactivity parameters a and v (Eq. 6; Eq. 22) derived from the best fit model solutions (Table 4) reveal important differences in apparent OM reactivity and its distribution on a global scale. Alongside a and v parameters compiled from the literature (Arndt et al., 2009; Boudreau and Ruddick, 1991; Contreras et al., 2013; Henkel et al., 2012; Mewes et al., 2016; Mogollón et al., 2012, 2016; Wehrmann et al., 2013; Ye et al., 2016), they provide useful constraints on the plausible range of a and v, as well as their control on the global variability in apparent OM reactivity. Thus, they provide important first order constraints for model parameterization in data poor areas.

Parameter v exerts a scaling influence on OM reactivity distribution. High v-values result in a high initial OM reactivity, whereas low v-values produce low initial reactivity (Arndt et al., 2013). For instance, an extremely low v-value of ≤ 0.01 for OM deposited during the late Cretaceous Oceanic Anoxic Event 2 at Demerara Rise (Arndt et al., 2009) has been linked to intense and rapid sulfurization of OM in the strongly euxinic subtropical Atlantic Ocean (Hülse et al., 2019), while previously published values for contemporary ocean sediments fall within the range 0.1 and 1.08 (Arndt et al., 2013; Boudreau and Ruddick, 1991). Inversely determined v values predominantly fall within the 0.1–0.2 interval (apparent 6^{th} – 11^{th} order of reaction), although lower and higher v values were also determined (Fig. 4a). They thus confirm the previously observed dominance of v values between 0.1 and 0.2 (Boudreau and Ruddick, 1991) and suggest that v is relatively constant across a

https://doi.org/10.5194/bg-2020-435
Preprint. Discussion started: 6 January 2021

wide range of different depositional environments encountered in the contemporary ocean. These findings are also in agreement with the parametrization of the empirically derived power law description of OM degradation (Middelburg, 1989) another continuum model, which applies a globally constant parameter of 0.16:

$$k(z) = 0.16 \cdot (a + age(z))^{-0.95} \quad (28).$$

Although the parameters of the so-called power model cannot be directly compared to those of the RCM due to different exponents, the RCM is nevertheless equivalent to a general power law with an exponent of –1:

$$k(z) = v \cdot (a + age(z))^{-1} \quad (29).$$

Thus, the v parameter range of the RCM is in good agreement with the 0.16 value imposed in the power law model.

Nevertheless, our results also reveal exceptions from this overall pattern. Particularly high v-values ($v > 0.25$) were determined for the Arabian Sea and Bering Sea. Similarly, Boudreau and Ruddick (1991) also report exceptionally high values ($v \approx 1$) for the Peru Margin and North Philippine Sea but attribute them to non-steady state depositional conditions. In our study, $v > 0.25$ also coincides in part with the poorest data-model fits, such that the robustness of such values is uncertain. Particularly in the Bering Sea, the high v-value (Table 4) might result from uncertainties associated with boundary conditions, as well as the transient features observed in the present-day TOC and SO_4^{2-} depth-profiles (e.g. Henkel et al., 2011; Hensen et al., 2003). However, model-derived $v > 0.25$ for the Arabian Sea agrees with previous diagenetic model results for that region. Luff et al. (2000) developed a 3G-model to investigate OM dynamics and found that bulk OM contains exceptionally reactive compounds with first order k of 0.2–30 y^{-1}. Additionally, Koho et al. (2013) observed high OM reactivity in the Arabian Sea sediments associated with anoxic bottom water conditions and a marked linear decrease in OM quality with an increase in bottom water oxygen concentrations. Likewise, Vandewiele et al. (2009) observed higher OM reactivity in sediments within the OMZ. Small scale differences in oxygen gradients at the SWI in Arabian Sea deposits have also been shown to affect the extent of post-depositional OM degradation (Bogus et al., 2012). Therefore, the somewhat atypical high v-values determined here (together with comparably low a-values; see below) for the Arabian Sea transect are realistic and indicate that those sediments receive an OM mixture containing exceptionally large fractions of highly reactive compounds (Koho et al., 2013; Luff et al., 2000; Vandewiele et al., 2009), which are quickly consumed at the SWI (i.e., rapid decrease in reactivity with burial). This is further supported by the high PP rates in the photic zone during Monsoon periods and efficient vertical transport of diatom and haptophyte detritus (Barlow et al., 1999; Cowie, 2005; Latasa and Bidigare, 1998; Shalapyonok et al., 2001) and deep carbon fixation by microorganisms (Lengger et al., 2019). Luff et al. (2000) showed that highly reactive OM in Arabian Sea sediments represents around 50–70% of the total OM fluxes at the SWI close to the continental margin, and it is composed mostly of fresh plankton, large aggregates, and faecal pellets. Further, the most reactive fraction is only present in

https://doi.org/10.5194/bg-2020-435
Preprint. Discussion started: 6 January 2021

the few uppermost millimetres of the sediment column. Thus, anoxic water conditions, associated with enhanced vertical OM fluxes within the OMZ enhance the burial of more reactive OM (e.g., Maerz et al., 2019; Zonneveld et al., 2010). In summary, our inversely determined v-values, alongside those compiled globally (Fig. 4a) and in addition to the empirically fitted power law parameter, reinforce the similarity of v values across a wide range of depositional environments, thereby providing an important first order constraint on model parametrization on the global scale.

Parameter a determines both the overall apparent reactivity, as well as the shape of the reactivity decrease with depth. High a-values result in an overall low OM reactivity, but a slow reactivity decrease with depth. In contrast, low a-values result in a higher reactivity, but also a more rapid decrease in reactivity with sediment depth (Arndt et al., 2013). Parameter a is often related to the degree of degradation (Arndt et al., 2013; Middelburg et al., 1993) and very fresh OM generally reveals very low a values ($a = 3.1 \cdot 10^{-4}$ y) (Boudreau and Ruddick, 1991; Westrich and Berner, 1984), while the heavily sulfurized OM deposited during Cretaceous Oceanic Anoxic Event 2 in the strongly euxinic subtropical Atlantic Ocean is characterized by very high a values ($a = 10^4$ y) (Arndt et al., 2009). Inversely derived a-values span several orders of magnitude (Table 4; Fig. 4b). They thus corroborate the high variability observed in previously published a-values compilations (e.g., Arndt et al., 2013; Boudreau and Ruddick, 1991) and suggest that parameter a exert the major control on the spatial variability in OM reactivity. Inversely determined a values also broadly agree with previously observed global patterns. Low values ($a < 10^2$ y; i.e. high apparent OM reactivity) are generally determined for depositional environments that are characterized by the rapid deposition of predominantly fresh, marine OM (e.g. Arabian Sea and shallow sites at the Northern European margin), while depositional settings that receive pre-degraded OM and/or complex mixtures of OM (e.g. Skagerrak) exhibit high a ($a > 10^3$ y). Between these endmembers, the inversely determined parameter a reveals a large variability that is further explored in the context of the respective depositional environments in Sect. 4.1.4. However, despite the large total range of inversely derived a-values which spans eleven orders of magnitude, most values fall into the range $10^0 < a < 10^4$ years, thus narrowing the most plausible interval of a-values. This is a valuable finding that can help better inform model parameterisation in data poor regions and timescales (e.g., Hülse et al., 2018).

4.1.3 OM reactivity distributions

The inversely determined parameters a and v not only provide insights into the initial apparent reactivity of the depositing OM but also allow the assessment of its evolution during burial. Here, we calculate the probability distribution of OM over k at the time of deposition on the SWI, as well as after burial at 10, 100, and 1,000 cmbsf (centimetres below seafloor). The distribution profiles (Fig. 5) reflect both a and v. Yet, it is important to note that changes in OM–k distributions with ongoing burial are not solely controlled by parameters a and v. Sedimentation rates ω also exert an impact on the degree of degradation since ω controls the residence time of OM at a distinct depth (and redox) horizon (i.e. the burial age; Eq. 7). Finally,

https://doi.org/10.5194/bg-2020-435
Preprint. Discussion started: 6 January 2021

degradation rates also depend on benthic OM contents (donor control) (Arndt et al., 2013). They thus also dictate changes in OM–k distribution with burial. Overall, high OM contents result in higher degradation rates. Therefore, the resulting changes in distribution reflect different exposure to heterotrophic degradation at similar burial depth. Since v-values are broadly similar across depositional settings, the differences in k distributions are mainly driven by the range of inversely determined a-values.

The Arabian Sea region (Fig. 5 j – l) is characterized by the deposition of highly reactive OM (highest v-values; Table 4). However, OM reactivity rapidly decreases with sediment depth (low a-values). The OM reactivity distributions show a clear depletion of the most reactive OM compounds in the uppermost 10 cm, resulting in a marked decrease in the overall reactivity over this depth, i.e., the k distributions shift towards lower values, in agreement with previous findings (Luff et al., 2000). Below 100 cmbsf the most reactive compounds have been degraded, and the remaining bulk OM is dominated by less reactive compounds ($k(z) < 10^{-5}$ y^{-1}). The inversely determined rapid decrease in OM reactivity can be explained with the often rapid deposition of predominantly marine OM (Cowie, 2005; Seiter et al., 2005), whose degradation during settling is limited by short residence times and/or locally anoxic conditions (Luff et al., 2000). The shallow, sub-oxic/anoxic sediments of the Northern European margin (Aarhus Bay – Fig. 5d; Arkona Basin – Fig. 5e) reveal a similar OM–k distribution and depth profile. However, the loss of the most reactive fractions within the uppermost 10 cm is less pronounced. This slowed decrease in OM reactivity with sediment depth could be due to the burial of terrestrial, yet reactive OM (Aquilina et al., 2010). In contrast, Skagerrak sediments (S10 – Fig. 5g; S13 – Fig. 5i) are characterised by the most homogeneous, albeit comparably unreactive OM mixture (high a-values; Table 4). The OM–k distributions reveal small changes from the SWI down to 1,000 cmbsf, reflecting a low overall reactivity, and thus low degradation rates. This somewhat surprising finding can be explained with the atypical character of the Skagerrak – a shallow environment that connects the brackish Baltic Sea with the saline North Sea and is characterized by an estuarine type circulation. Due to this circulation pattern, the Skagerrak acts as the final sink for marine OM produced in the North Sea (Lohse et al., 1995; Van Weering et al., 1987). As a consequence, more than 90% of the OM that is deposited in the Skagerrak is derived from re-suspended and pre-degraded marine OM or terrestrial OM (ca. 20% of the OM buried) (de Haas and van Weering, 1997) of generally low quality (Dauwe et al., 1999a, 1999b).

Between those two endmember cases (high reactivity Arabian Sea and low reactivity Skagerrak), sediments from other sites generally reveal small changes in the continuous OM–k distributions within the uppermost 10 cm. At all sites, below 100 cmbsf k-values have converged to < 10^{-4} y^{-1}, since $age(z) >> a$ (see Eq. 23), and thus dominates k-values at great depths. As such, only the least reactive fractions are preserved, leading to an overall low OM reactivity in deeper sediments that is largely independent of the initial apparent OM reactivity $k(0)$. Sediments from the Bering Sea (Fig. 5m) are a notable exception. OM reactivity decreases gradually throughout the sediment column, reflecting both unusually high a and v values (Table 4). The Bering Sea is one of the most productive ocean regions and OM deposition is mostly fuelled by spring and summer blooms (Coyle et al., 2008; Stabeno and Hunt, 2002; Stockwell et al., 2001). However, due to great water depths and

https://doi.org/10.5194/bg-2020-435
Preprint. Discussion started: 6 January 2021

low sedimentation rates, OM can experience extensive ageing and pre-processing prior to burial and result in the OM distribution pattern observed here (Fig. 5m). The heterogeneous distribution of the Bering Sea OM is, to a certain extent, comparable to that observed in the Arabian Sea region (Fig. 5 j – l). However, there is a fundamental distinction in the downcore evolution of OM–k distributions at these contrasting regions that is driven by the magnitude of a-values (Table 4), as well as timescales (Table 1).

4.1.4 Emerging environmental patterns in OM reactivity

Inverse model results reveal that parameter a exerts the main control on the global variability in apparent OM reactivity, but also highlight the large range of plausible values spanning several orders of magnitude (Fig. 2b, Table 4). Our ability to quantify and predict benthic OM dynamics strongly depends on a general framework that allows the constraint of parameter a when observational data is scarce or unavailable (e.g. global, future and past model scenarios). The need for such a general framework has been recognized since the early days of RTM. Based on the rationale that the reactivity of OM settling onto the sediment is controlled by the degree of degradation, and thus its residence time in the oxygenated water column, early efforts have explored correlations between OM reactivity and water depth, sedimentation rate or OM fluxes (Boudreau, 1997; Boudreau and Ruddick, 1991; Müller and Suess, 1979; Tromp et al., 1995). However, the derived relationships were based on limited datasets and a more recent compilation of global data did not reveal statistically significant correlations between OM reactivity and single depositional environmental descriptors (Arndt et al., 2013). That global compilation, however, combined OM degradation model parameters derived from structurally different models and using observational data of different complexity, thus somewhat compromising their comparability. Therefore, we further explore these links combining our newly generated dataset with those compiled from previously published RCM parameters (Fig. 6).

In agreement with the previous global assessment (Arndt et al., 2013), we do not find any significant correlation between the reactivity parameters (a and $k(0)$) and master characteristics of depositional environments, as proposed for k–ω (Boudreau, 1997; Tromp et al., 1995), k–F_{OM} (Boudreau, 1997; Müller and Suess, 1979), and a–ω (Boudreau and Ruddick, 1991). These results, therefore, further confirm that the spatial variability in a and thus apparent OM reactivity is not determined by one single characteristic of the depositional environment but is the result of a complex and dynamic interplay of multiple environmental controls. However, despite the large scatter, very broad trends that generally agree with previously proposed relationships emerge (Fig. 6). Depositional environments that are characterised by low sedimentation rates, low OM fluxes, or great water depths generally display high a-values (i.e. low apparent reactivity), whereas settings characterized by high sedimentation rates, high OM fluxes, or shallow water depth generally display lower a-values (high apparent reactivity). While these trends are extremely weak on a global scale, they are relatively more pronounced within a given depositional environment (i.e. on a local/regional scale). Despite the lack of clear global relationships between apparent OM reactivity and one

https://doi.org/10.5194/bg-2020-435
Preprint. Discussion started: 6 January 2021

environmental master variable, general but, not significant correlations between OM reactivity and single environmental controls can be identified within a given environment.

Inverse model results show that water depth seems to be a useful and easily accessible first-order proxy for the complex interplay of environmental controls on OM reactivity. At the global scale, inversely determined apparent OM reactivity for the deep, well-oxygenated sites in the Bering Sea and Argentine Basin fall in the lower end of the reactivity spectrum. Here, the prolonged exposure to oxygen (Hartnett et al., 1998) and pelagic degradation (Cram et al., 2018; Maerz et al., 2019; Müller and Suess, 1979; Weber et al., 2016), as well as the continuous ageing during settling (Griffith et al., 2010), contribute to the determined low apparent OM reactivity in the Argentine Basin (e.g., Riedinger et al., 2005, 2014, 2017) and Bering Sea. In contrast, shallow coastal environments, such as the Northern European region, reveal generally higher apparent OM reactivities. In addition to this weak global trend, regional k–h reactivity trends emerge. For instance, the Northern European region, inversely determined apparent OM reactivity generally decreases (i.e. increase in a,) with increasing water depth (Fig. 6 b,e). A notable exception to this regional trend is the comparably low OM reactivity determined for the Severn estuary. The Severn estuary is characterized by one of the largest tidal ranges on Earth resulting in pronounced environmental gradients along the dynamic land-ocean transition. OM of terrestrial, anthropogenic and marine sources not only mix along the gradient but also interact with high loads of fine, suspended particular material. In addition, intense, tidally driven deposition-resuspension cycles (Dyer, 1984; Jonas and Millward, 2010; Manning et al., 2010; Uncles, 2010) result in a continuous re-exposure of benthic OM, which might cause the lower apparent reactivity of the buried OM. Similar to the Northern European region, the Rhone delta transect, also reveals a decrease in apparent OM reactivity with an increase in water depths from the proximal zone to the shelf (Fig. 6e). This general trend is supported by the previously observed decrease in OM quality recorded by individual OM fractions (Pruski et al., 2015), as well as the ageing of bulk OM across the Rhone shelf (Cathalot et al., 2010). However, the weak trends and numerous exceptions at both global and regional level caution against the uncritical use of such simplistic relationships. Our findings suggest that further important additional controls often complicate and sometimes inhibit the use of water depth as a predictor for apparent OM reactivity. For instance, the Arabian Sea is a notable exception from the general global trend observed between OM reactivity and water depth due to the presence of the pronounced OMZ (e.g. Bogus et al., 2012; Fischer et al., 2012). Here, reactivity is 2–3 orders of magnitude higher than those derived for other deep-sea sites. Reactivity is rather comparable to reactivities determined for shallow sites in the Northern European margin and the Rhone delta. Across the Arabian Sea OMZ transect, only a modest regional depth trend is observed, with a decrease in reactivity (i.e. increase in a) from the OMZ to increasing water depths and bottom water oxygen concentrations (Cowie, 2005; Luff et al., 2000). While distinct from the overall k–h discussed above, the Arabian Sea OMZ region exhibit relatively similar patterns to other high productive, anoxic water column systems, e.g., Peru margin (Boudreau and Ruddick, 1991), Blake ridge (Marquardt et al., 2010; Wallmann et al., 2006), as well as California, Chile, Costa Rica, and Namibia margins (Marquardt et al., 2010). This suggests a general separation from anoxic and oxic water columns shaping benthic OM reactivity.

https://doi.org/10.5194/bg-2020-435
Preprint. Discussion started: 6 January 2021

705

Inversely determined apparent OM reactivities reveal that the use of sedimentation rates are poor proxies for the complex interplay of environmental controls on OM reactivity (Fig. 6 c,f). For instance, sediments from the Northern European margin experience similar depositional rates but reactivity spans several orders of magnitude, suggesting the weak control imposed by sedimentation rates on OM reactivity (e.g., Arndt et al., 2013). This could partly be due to strong contribution of
710 remobilized, pre-degraded OM and mineral protection in the Skagerrak sediments (Mayer, 1994a, 1994b), as well as the higher OM fluxes onto shallow, sub-oxic/anoxic sediments of the Northern European margin, like Aarhus Bay (Dale et al., 2008b) and Arkona Basin (Mogollón et al., 2012). Similarly, in the Arabian Sea the absence of relationships between reactivity and sedimentation rates is likely to be associated to high fluxes of unprocessed OM within the OMZ (Cowie, 2005; Luff et al., 2000) and enhanced OM mineral protection outside of the OMZ (Keil and Cowie, 1999). In contrast, across the Rhone seaward
715 transect a decrease in sedimentation rates is followed by an increase in a, and thus a decrease in apparent OM reactivity k. At the proximal zone, the sedimentary OM deposition is characterised by terrestrial sources and aquatic PP, which is highly reactive. In contrast, at the shelf area, the major source of OM is marine PP (Pozzato et al., 2018). Here, slow settling through the water column allows longer exposure of OM to heterotrophic degradation prior to burial, resulting in an overall decrease in OM reactivity (e.g., Middelburg et al., 1997), whereas at shallow depths with great sedimentation rates the burial of reactive
720 OM is favoured. Additionally, there is evidence of strong OM–mineral association, and thus mineral protection in the Rhone shelf sediments (Mayer, 1994a, 1994b), which results in decreased reactivity. Our findings thus suggest that sedimentation rates might be useful predictors of reactivity across strong environmental gradients like those generally observed in land-ocean transition systems (e.g., Epping et al., 2002). In other environments, additional and more dominant controls on OM reactivity blur the use of sedimentation rates in other environments.

725

4.2 Influence of OM reactivity on benthic-pelagic coupling

OM degradation is the engine behind the complex and dynamic interplay of diagenetic processes in marine sediments. Consequently, the quantity and quality of the deposited OM exerts an important control on benthic-pelagic coupling processes with potential implications on global biogeochemical cycles and climate. While the influence of OM quantity on benthic-
730 pelagic exchange across a range of depositional environments has been previously assessed (Krumins et al., 2013; Soetaert et al., 1996, 1998; Thullner et al., 2009), these assessments made simplified assumptions about the variability of apparent OM reactivity. Consequently, the role of reactivity on benthic-pelagic fluxes remains poorly quantified. Therefore, we further explore the influence of differences in OM reactivity on OM degradation rates and their respective metabolic pathways, AOM dynamics, as well as benthic fluxes across all study sites.

735

https://doi.org/10.5194/bg-2020-435
Preprint. Discussion started: 6 January 2021

4.2.1 Control of OM reactivity on OM degradation rates and respiration pathways

Depth-integrated (0–10,000 cmbsf) OM degradation rates (ΣR_C; Eq. 24) mirror the large spatial variability in apparent OM reactivity (i.e. parameter a) across depositional environments. However, results show a strong correlation of ΣR_C with OM fluxes (Fig. 7a, $r^2 = 0.97$; $p < 0.01$; $n = 14$), thus confirming previous findings by Henrich (1992) who showed that high depth-integrated heterotrophic OM degradation rates strongly correlate with high F_{OM} (typically reactive OM). Together with the fact that k does not show any systematic relationship with F_{OM} (Fig. 6g), as previously suggested (Boudreau and Ruddick, 1991; Müller and Suess, 1979) and that apparent reactivity often converges towards similar values in deeper sediments (see Sect. 4.1.3 OM reactivity distributions), these findings indicate that the magnitude of the OM deposition flux rather than its quality often exerts a first order control on depth-integrated rates of OM degradation. The Arabian Sea region follows that general trend with high ΣR_C and high F_{OM}; however, these high depth-integrated rates are driven by exceptionally high OM reactivities (i.e. high v) rather than high F_{OM}. As previously discussed, the combination of high PP rates and the presence of a well-developed OMZ delivers and preserves fresh, reactive OM to and within the sediments, where intense heterotrophic degradation takes place, consuming up to 70% of the most reactive compounds in the uppermost few millimetres of the sediment (Cowie, 2005; Koho et al., 2013; Luff et al., 2000; Rixen et al., 2019; Vandewiele et al., 2009). Model results thus indicate that, while F_{OM} exerts a dominant control on depth-integrated OM degradation rates across most depositional environments, apparent OM reactivity becomes a dominant control in depositional environments that receive exceptionally reactive OM.

Overall, rates of OM degradation coupled to consumption of oxygen (aerobic OM degradation pathway) and nitrate (denitrification) make a small relative contribution (< 10%) to total degradation rates in the investigated depositional environments (Rhone proximal zone, Skagerrak, Bering Sea, and Argentine Basin; Fig. 7b) due to their overall dynamic nature that favours the dominance of organoclastic sulfate reduction (Bowles et al., 2014; Jørgensen and Kasten, 2006; Thullner et al., 2009), and the length of sediment column (1,000 cmbsf) integrated for those estimates. The contribution of the aerobic OM degradation pathway further decreases with a decrease in OM apparent reactivity (i.e. increase in a), whereas the contribution of denitrification increases. This pattern can be explained by the fact that highly reactive (i.e. low a) OM is predominantly degraded in the uppermost sediment layers, thus increasing the relative contribution of oxygen, if oxygen is the dominant electron acceptor at these sediment depths (Freitas et al., 2020; Glud, 2008). In contrast, a decrease in apparent reactivity leads to a higher burial of OM to sub-oxic or anoxic sediments (e.g., Meister et al., 2013). In addition, in this case, the enhanced production of reduced species at depth further decreases the relative contribution of the aerobic OM degradation pathway to overall OM degradation rates by channelling more oxygen consumption through the re-oxidation of reduced species (e.g., ammonium and hydrogen sulfide) that diffuse up to shallower sediment layers (Glud, 2008). Here, we do not consider the degradation pathways mediated by metal oxides due to a lack of SWI data that would allow constraining boundary conditions of metal oxides. While this might result in a slightly overrepresentation of sulfate reduction (e.g., at the Skagerrak;

https://doi.org/10.5194/bg-2020-435
Preprint. Discussion started: 6 January 2021

Canfield et al., 1993; Rysgaard et al., 2001), it has been demonstrated that metal oxide pathways represent a minor contribution to total OM heterotrophic degradation on a global scale (Freitas et al., 2020; Thullner et al., 2009), albeit in continental margin sediments iron hydroxide reduction may represents an important OM degradation pathway (Beckler et al., 2016).

It has been suggested that anoxic metabolic pathways represent significant pathways of OM degradation (e.g., Bowles et al., 2014; Jørgensen and Kasten, 2006; Thullner et al., 2009). Our results show that sulfate reduction is the main oxidative pathway in regions characterised by high apparent OM reactivity ($a < 10^2$ y) and intermediate OM fluxes ($F_{OM} \sim 10^{-4}$–10^{-3} mol C cm^{-2} y^{-1}), e.g., the Arabian Sea region (e.g., Cowie, 2005; Luff et al., 2000), the Arkona Basin and Aarhus Bay (e.g., Dale et al., 2008b; Jørgensen et al., 2019a; Mogollón et al., 2012). Here, the rapid degradation of highly reactive OM compounds takes place in shallower sediment layers where sulfate can be efficiently replenished by exchange with bottom waters. In addition, high relative contributions of sulfate reduction are also simulated for environments that are characterized by a reduced supply of less reactive ($a > 10^3$ y) OM deposition fluxes , such as the Argentine Basin and Bering Sea sites (e.g., Hensen et al., 2003). Here, the lower quantity ($F_{OM} < 10^{-5}$ mol C cm^{-2} y^{-1}) and quality ($k < 10^{-5}$ y^{-1}) of OM supplied to the sediment allows for a deeper sulfate penetration (Fig. 3 m-n), thus sustaining sulfate reduction over a greater sediment volume (e.g., Bowles et al., 2014; Meister et al., 2013; Riedinger et al., 2005, 2014, 2017). In contrast, methanogenesis is an important degradation pathway in environments that are characterized by a high supply ($F_{OM} > 10^{-3}$–10^{-2} mol C cm^{-2} y^{-1}) of both highly reactive ($a = 10^0$–10^1 y) OM (Rhone proximal zone and Helgoland Mud Area, North Sea), as well as less reactive ($a > 10^3$ y) OM (Skagerrak). In the first case, fast burial of reactive OM drives the development of a shallow methanogenic zone in the sediment (shallow sulfate penetration; Fig. 3 b,f) (e.g. Aromokeye et al., 2020; Oni et al., 2015a, 2015b; Rassmann et al., 2020), whereas in the latter case low reactive OM escapes sulfate reduction and is degraded deeper in the sediment via methanogenesis (e.g., Dale et al., 2008a; Knab et al., 2008; Meister et al., 2013). In both cases, the produced methane diffuses up and supports an enhanced consumption of sulfate through AOM (Sect. 4.2.2). As a result, the sulfate available at depth is mostly channelled to AOM instead of organoclastic sulfate reduction (e.g., Bowles et al., 2014; Niewöhner et al., 1998; Regnier et al., 2011; Jørgensen and Kasten, 2006; Jørgensen et al., 2019a; Riedinger et al., 2005, 2014, 2017).

Our model results highlight that OM reactivity exerts a dominant control on the relative significance of OM degradation pathways. Additionally, OM deposition fluxes control the amounts of material delivered to the respective redox layers, as well as the timescale of burial which influences the apparent OM reactivity at depth (Eq. 26). This has important implications for carbon burial on geological timescales since depositional regimes with fast burial rates favour the escape of OM from thermodynamically more favourable metabolic pathways to methanogenesis. In these settings, sulfate and oxygen (if available) are predominantly channelled to the re-oxidation of reduced species produced during OM breakdown, with important implications for authigenic mineral precipitations (e.g. Arndt et al., 2009; Bahr et al., 2009; Henkel et al., 2012; Nöthen and Kasten, 2011; Pierre and Fouquet, 2007; Sun and Turchyn, 2014; Wehrmann et al., 2013), isotopic signatures (e.g. Ussler and

https://doi.org/10.5194/bg-2020-435
Preprint. Discussion started: 6 January 2021

Paull, 2008; Zhou et al., 2016) and benthic alkalinity fluxes (e.g. Łukawska-Matuszewska and Graca, 2018; Rassmann et al., 2020; Snyder et al., 2007; Soetaert et al., 2007).

4.2.2 Anaerobic oxidation of methane dynamics

Marine sediments represent the largest pool of methane in the global carbon cycle. However, up to 90% of CH_4 produced in marine sediments is anaerobically oxidised via sulfate reduction (Jørgensen et al., 2019b; Puglini et al., 2020; Regnier et al., 2011). AOM not only represents an efficient benthic CH_4 sink, it also exerts an important influence on the balance between organoclastic sulfate reduction and methanogenesis (Jørgensen et al., 2019b; Jørgensen and Kasten, 2006) and has important implications for benthic alkalinity fluxes (e.g. Krumins et al., 2013; Snyder et al., 2007; Soetaert et al., 2007) and authigenic carbonate dynamics (e.g. Bahr et al., 2009; Nöthen and Kasten, 2011; Pierre and Fouquet, 2007; Sun and Turchyn, 2014; Ussler and Paull, 2008). AOM occurs at the sulfate-methane transition (SMT), a narrow zone where non-zero SO_4^{2-} and CH_4 concentrations overlap (e.g., Jørgensen and Kasten, 2006; Meister et al., 2013; Niewöhner et al., 1998; Regnier et al., 2011). The depth of the SMTZ can vary from cm (e.g. Dale et al., 2008a; Jørgensen et al., 2019a; Knab et al., 2008; Mogollón et al., 2012; Oni et al., 2015a, 2015b) to hundreds of meters (e.g. Arndt et al., 2009; Wehrmann et al., 2013) as a function of different environmental controls such as, among others, OM quantity and quality, sedimentation rate, active fluid flow, or microbial growth dynamics (Puglini et al., 2020; Regnier et al., 2011). Reflecting the diversity of the depositional environments studied here, we observe a broad range of SMTZ depths (Fig. 8 a-c). Generally, we observe a deepening of the SMTZ with decreasing sedimentation rates, which agrees with global patterns (Egger et al., 2018). Not surprisingly, the controls on both AOM depths and overall rates emerge from a combination of environmental forcing.

Confirming previous findings (Egger et al., 2018; Regnier et al., 2011) and in line with the dominant influence of OM reactivity on benthic redox zonation, OM reactivity exerts a significant influence on the depth of the SMTZ (Fig. 8b) and the depth-integrated AOM rates (Fig. 8d). The lowest ΣAOM and deepest SMTZ depths are determined for the low apparent OM reactivity sites in the deep-sea, well oxygenated bottom waters regions (Table 4). In those regions, low OM reactivity results in low rates of heterotrophic degradation (Fig. 7a) and, thus, deep SO_4^{2-} penetration (Fig. 3 m–n) or no SO_4^{2-} depletion at all. In contrast, sediments from the Helgoland Mud area, North Sea, are characterized by a shallow SMTZ and intense ΣAOM (Oni et al., 2015a, 2015b). High OM reactivity in combination with high depositional fluxes (Fig. 8 b–e) result in the complete depletion of TEAs in the upper sediment (z < 50 cm), and thus allows the establishment of methanogenesis at relatively shallow sediment depth. However, high OM reactivity not always results in shallow SMTZ and intense AOM rates. Associated with moderate depositional fluxes, high apparent OM reactivity reduces the amount of reactive OM that reaches the methanogenic zone, and thus causes a deepening of the SMTZ and a decrease in ΣAOM. Such a pattern can be observed at the shallow, sub-oxic/anoxic sediments from the Aarhus Bay (Flury et al., 2016) and Arkona Basin (Mogollón et al., 2012) sites. Here, high OM reactivity (a < 10^1 y) supports high rates of degradation close to the SWI (Fig. 7a) where SO_4^{2-} is constantly replenished

https://doi.org/10.5194/bg-2020-435
Preprint. Discussion started: 6 January 2021

from bottom waters and limits OM fluxes to the deeper, methanogenic sediment (e.g., Flury et al., 2016; Meister et al., 2013; Regnier et al., 2011). For moderate depositional fluxes, associated with lower OM reactivity ($a > 10^2$ y) such as determined for the Skagerrak sites a shoaling of the SMTZ and higher ΣAOM are simulated (Dale et al., 2008a; Knab et al., 2008). The pre-degraded OM buried in Skagerrak sediments (Aquilina et al., 2010) is predominantly degraded via methanogenesis (Fig. 7b). Our results thus show that OM reactivity exerts an important control on SMTZ depths and AOM rates. Depositional environments that are characterized by the deposition of OM of intermediate reactivity, as well as those that receive high fluxes of highly reactive OM reveal a shallow SMTZ and high AOM rates, whereas AOM is substrate limited in environments that receive low amounts of highly reactive material or that are characterised by the deposition of less reactive OM.

4.2.3 OM reactivity controls on sediment-water interface fluxes patterns

Model results show that apparent OM reactivity exerts an important control on OM degradation and benthic redox zonation and, consequently, nutrient recycling at the seafloor. Here, we estimate benthic-pelagic fluxes based on our model-derived concentration depth profiles of dissolved species (O_2, NO_3^-, SO_4^{2-}, NH_4^+, and PO_4^{3-}). We emphasise that these flux calculations are based on simulated depth profiles at steady-state and are thus only weakly affected by sampling limitations. Uncertainties in SWI concentrations and upper boundary conditions are induced by the common loss of the uppermost sediment layers during sampling with gravity and piston corers. Multi-corers and benthic landers are more suitable sampling devices for SWI assessments since such methods usually recover the undisturbed uppermost sediments, allowing for a better quantification of concentration depth profiles near the SWI (e.g. Hensen et al., 2006). Despite of such limitations, our model-derived flux estimates across the SWI allow us to investigate the links between nutrient recycling and OM reactivity and to assess qualitative differences across sites.

We observe that OM reactivity broadly controls the spatial patterns of benthic-pelagic fluxes, as well as the relative importance of different transport processes (Fig. 9). Overall, molecular diffusion is the main transport pathway (Fig. 9 f–j). However, the relative importance of bioirrigation increases at environments characterized by low deposition of less reactive OM. This occurs because of relative the decrease in diffusive fluxes as a consequence of weak concentration gradients across the SWI. Bioturbation fluxes are generally low and reflect our assumption of depth-dependent D_{bio} (Middelburg et al., 1997). Advective fluxes become an important transport mechanism driving downward sulfate fluxes, especially in rapidly accumulating sediments, as well as at sites characterized by low OM reactivity and moderate depositional rate.

Overall, a high apparent OM reactivity, and thus high rates of OM degradation (Fig. 7a), especially at shallow sediment depth, drive high uptake fluxes of dissolved TEA (Fig. 9 a–c). Sulfate uptake dominates the benthic TEA uptake, particularly at sites where oxygen and nitrate are unavailable TEA (Fig. 9c), due to the dominance of sulfate reduction across sites. Sulfate uptake fluxes increase with an increase in apparent OM reactivity. Oxygen and nitrate fluxes follow a similar trend. For instance, at

https://doi.org/10.5194/bg-2020-435
Preprint. Discussion started: 6 January 2021

the Rhone proximal zone unusually high sedimentation rates (Pastor et al., 2011), which delivers fresh and highly reactive OM (Cathalot et al., 2010; Pruski et al., 2015) support high F_{OM} and ΣR_C (Fig. 7a; Table 4), thus promoting intense oxygen consumption at the SWI (Rassmann et al., 2016) that are driven by both the aerobic degradation of OM, as well as the re-oxidation of reduced species (see Table S1 for a reaction network review). Similarly, high degradation rates result in an increased nitrate demand for denitrification. Thus, the high input of highly reactive OM ($k > 10^{-2}$ y^{-1}; Table 4) yields high rates of aerobic degradation of OM and denitrification, and consequently intense downward oxygen and nitrate fluxes. Similarly, in the Arabian Sea sediments below the OMZ the high input of fresh phytoplankton debris (Cowie, 2005; Koho et al., 2013; Rixen et al., 2019; Vandewiele et al., 2009) and potentially chemoautotroph biomass (Lengger et al., 2019) associated to intense degradation rates in the uppermost sediment layers (Luff et al., 2000), result in a high relative contribution of aerobic degradation of OM and denitrification to total OM oxidation. Consequently, both benthic oxygen and nitrate uptake fluxes are comparably high. In contrast, at regions characterised by deposition of less reactive OM ($k < 10^{-4}$ y^{-1}; Skagerrak, Argentine Basin, and Bering Sea), benthic-pelagic fluxes of oxygen, nitrate, and sulfate are generally low. The low degradation rates in these regions result in low TEA consumption at the SWI.

Benthic fluxes exert a crucial role in nutrient recycling. In the Arabian Sea region, large phytoplankton blooms are associated to monsoon conditions, which result in upwelling of nutrient-rich bottom water (SW monsoon) and deepening of the mixed-layer (NE monsoon) (Cowie, 2005; Luff et al., 2000; Rixen et al., 2019). Similarly, across the Northern European margin, spring and summer diatom blooms are common (Fleming-Lehtinen and Laamanen, 2012; Jensen et al., 1990; Karlson et al., 1996; Lomstein et al., 1990; Wiltshire and Manly, 2004) and maintained by benthic nutrient fluxes. Additionally, bottom water upwelling and nutrient recycling is an important mechanism sustaining spring and summer PP at the Bering Sea (Coyle et al., 2008). Benthic ammonium and phosphate recycling fluxes mirror the reactivity and OM degradation patterns (Fig. 9 d–e). The largest fluxes are determined for the Arabian Sea region, as well as the shallow Aarhus Bay and Arkona Basin, where the deposition of highly reactive OM drives intense degradation close to the SWI (Table 4). In contrast, the lowest nutrient recycling fluxes are observed in regions characterized by the deposition of less reactive OM (phosphate fluxes are negligible at Skagerrak sites S10 and S13), where heterotrophic degradation rates are slow (e.g., Colombo et al., 1997; Griffith et al., 2010; Hartnett et al., 1998; Hensen et al., 2000; Sun and Wakeham, 1994; Wakeham et al., 1997).

5. Conclusions

We developed and applied an inverse modelling approach to quantify apparent OM reactivity (i.e. parameters a and v) based on a common minimum set of benthic observational data, as well as a common RTM approach for 14 different sites across five different depositional environments.

https://doi.org/10.5194/bg-2020-435
Preprint. Discussion started: 6 January 2021

Our results provide important first-order constraints on model parameterization that can inform on the choice of parameter values in data poor areas, as well as global model applications and past and future model scenarios. They corroborate previous findings (Arndt et al., 2013; Boudreau and Ruddick, 1991) that the RCM parameter v is globally relatively constant (v = 0.1–0.2). Exceptionally high v > 0.2 are associated to particular cases, like the deposition and burial of highly reactive phytoplankton debris in high productivity regions associated with well-established OMZs, e.g., the Arabian Sea and the Peruvian shelf. In contrast, we show that the RCM parameter a can span several orders of magnitude at a global scale. Such a large variability is linked to a combination of multiple environmental drivers that control the quality of OM delivered to sediments, as well as the timescale of settling and burial, and thus exposure to favourable oxic conditions and ageing. These findings suggest that the parameter a exerts the main control on the variability of apparent OM reactivity, and that future modelling efforts to quantify OM reactivity on a global scale could thus be reduced to one main reactivity variable. Based on inverse model results, we narrowed the most plausible range of a to 10^0–10^4 years. This is a valuable constraint when dealing with data poor regions and timescales (e.g., Hülse et al., 2018), since it excludes extreme values at both ends of the a-range. In addition, inverse model results further confirm the notion that apparent OM reactivity is controlled by a complex and dynamic interplay of environmental drivers, which are measurable and allow the quantification of a, v, and k. They caution against the use of single environmental master variable such as water depth, sedimentation rate or organic matter deposition fluxes beyond the local scale. Instead, they call for a more holistic, interdisciplinary exploration of OM reactivity in its entire environmental context. Such integrative assessments are key to mechanistically understanding benthic carbon and nutrient dynamics.

Model results reveal that OM deposition fluxes exert a first-order control on total depth-integrated rates of OM degradation, except at settings that receive exceptionally highly reactive OM fluxes (e.g., the Arabian Sea OMZ region), and OM degradation rates are most intense in the uppermost sediment depths (z < 50 cmbsf). Yet, our model results highlight the important role of apparent OM reactivity in controlling the relative significance of different metabolic pathways, redox zonation of the sediment, the rate of AOM, as well as benthic TEA uptake and nutrient recycling fluxes. The fluxes of dissolved species across the SWI are strongly coupled to OM turnover, which is driven by reactivity. Particularly, the release of macronutrients (e.g., ammonium and phosphate) back to pelagic systems seems to be closely linked to reactivity patterns. The benthic-pelagic fluxes have a crucial impact on sustaining PP in regions characterised by the occurrence of spring and summer phytoplankton blooms, e.g., the Northern European margin, the Arabian Sea, and the Bering Sea. Alongside TEA availability and burial fluxes, OM reactivity regulates oxidative pathways and the predominance of anaerobic degradation of OM even at shallow sediment depths. In particular, the balance between organoclastic sulfate reduction and methanogenesis, and consequently the development of AOM, is strongly influenced by OM reactivity patterns.

Our findings have direct implications on the constraints for OM burial and preservation over long timescales. OM buried deeper than 100 cmbsf is expected to be predominantly of extremely low reactivity, which progressively becomes

https://doi.org/10.5194/bg-2020-435
Preprint. Discussion started: 6 January 2021

thermodynamically unfavourable as an energy source for microbial processing (e.g., Arndt et al., 2013; LaRowe et al., 2020b). Thus, the overall low reactivity character of OM in deeply buried sediments results in carbon sequestration at geological timescales. The processes leading to the preservation of highly unreactive OM are mostly attributed to selective degradation during settling and burial (Zonneveld et al., 2010) and mineral protection (Hemingway et al., 2019), and possibly sulfurization (Hülse et al., 2019; Sinninghe Damsté et al., 1988, 1998). Therefore, systematically understanding the processes driving OM burial and carbon removal from active pools (e.g., atmosphere, soils, pelagic systems, and surface sediments) can help us to better constrain uncertainties associated to perturbations to the carbon cycle and climate. Thus, our findings demonstrate that OM reactivity and its underlying environmental drivers are crucial components of carbon immobilisation over long/geological timescales.

Altogether, our inverse model results not only provide first, important constraints on model parametrization and a first step towards a general framework for model parameterization, but also help elucidate how changes in environmental conditions can affect benthic biogeochemical cycling and the role of marine sediments as a long-term carbon sink, and consequently their significance in the past, present and future feedback of the climate system.

https://doi.org/10.5194/bg-2020-435
Preprint. Discussion started: 6 January 2021

Acknowledgements

FSF was supported by a PhD scholarship from the Science without Borders Programme (Ciência sem Fronteiras), sponsored by the CAPES Foundation within Ministry of Education, Brazil, grant number 9999.009541/2013-06. FSF also thanks funding from the UKRI Natural Environment Research Council (NERC), grant number NE/P006493/1 (Changing Arctic Ocean Seafloor – ChAOS). RDP acknowledges the advanced ERC grant 'The greenhouse earth system' (T-GRES, project reference 340923) and the Royal Society Wolfson Research Merit Award. SA and PAP acknowledge funding from the European Union's Horizon 2020 research and innovation programme under the Marie Sklodowska-Curie grant agreement number 643052 745 (C-CASCADES). ST PhD was funded by a President's Scholarship, Cardiff University. CR and JR were supported by the INSU/EC2CO program MissRhoDia and by the French state program "Investissement d'avenir" run by the National Research Agency (AMORAD project ANR-11-RSNR-0002).

Authors contributions

FSF, SA, and RDP designed this study. PAP developed and implemented changes to model description (multi-G approximation of the RCM). SK, BBJ, JR, CR, ST, and HS provided porewater and sediment data to inform model experiments and contributed to discussing and interpreting the data and model results. FSF compiled data, ran all model simulations, and performed data-model integration. FSF wrote the manuscript with significant contributions from SA. All co-authors edited and approved the manuscript.

Code/data availability

The model code is available at the GitHub repository (https://github.com/felipesalesdefreitas/BG_2020_435). The data is available on PANGAEA database (www.pangaea.de) where indicated, or at cited literature along the manuscript.

Competing interests

The authors declare no conflicts of interest.

https://doi.org/10.5194/bg-2020-435
Preprint. Discussion started: 6 January 2021

Biogeosciences Discussions Open Access EGU

Table 1. Oceanographic context of depositional environments studied in the large-scale organic matter reactivity quantification.

	Geographical properties			*Physical properties*			*Organic matter characteristics*				*Biological properties*		*Reference*
	Site **Core ID**	**Lat (°)** **Lon (°)**	**Köppen climate zone** (Chen and Chen, 2013)	**Setting** **Depth (m)**	**Sed. rate (cm y^{-1})** **Bottom temp. (° C)**	**SWI redox condition**	**Benthic province** (Seiter et al., 2004)	**TOC (wt%)** **OC:SA (mg m^{-2})**	**$\Delta^{14}C$ (‰)** **F_{mod}**	**Type** **Input**	**Bioturbation activity**	**Ecosystem structure**	
A	Severn estuary ST-1	51.50 N 3.07 W	Temperate (Cfb)	Coast 8	$4.3 \cdot 10^{-1}$ 18.0	Sub-oxic	EUR1	3.0 N/A	N/A N/A	Largely Terrestrial Fluvial	Non-Bioturbated	Restrict phytoplankton community due to high turbidity. Microphytobenthos (mainly diatoms; but also, green algae, euglenophytes, and cyanobacteria) contributes to most of PP in tidal flats and shallow environments, with high spatial heterogeneity.	(Langston et al., 2010; Thomas, 2014; Underwood, 2010)
B	Rhone proximal zone A	43.31 N 4.85 E	Temperate (Cfb) / Mediterranean (Csa/Csb/Csc)	Coast 19	$1.0 \cdot 10^{1}$ 15.0	Oxic	EUR2	2.0 N/A	143 ± 14 N/A	Largely terrestrial and aquatic Fluvial	Bioturbated	Coccolithophorids are dominant year-round. During spring blooms, diatoms peak and dominates over cyanobacteria.	(Cathalot et al., 2010; Mayer, 1994b; Pastor et al., 2011; Pozzato et al., 2018; Rassmann et al., 2016, 2020; Uitz et al., 2012)
C	Rhone shelf C	43.27 N 4.77 E	Temperate (Cfb) / Mediterranean (Csa/Csb/Csc)	Shelf 74	$5.0 \cdot 10^{-1}$ 14.0	Oxic	EUR2	1.3 0.4 – 0.7	−218 ± 9 N/A	Mixed terrestrial and marine Fluvial and marine PP	Bioturbated		
D	Aarhus Bay 173GC 174GC	56.11 N 10.34 E	Temperate (Cfb)	Coast 15	$3.2 \cdot 10^{-1}$ 9.0	Sub-oxic or anoxic during summer	EUR1	3.5 N/A	N/A N/A	Largely terrestrial with marine contribution in the surface sediments Fluvial and marine PP	Bioturbated	Stable stratification separates an upper, low salinity, oligotrophic water mass from lower, high salinity, nutrient replete waters. In the upper layer, mixotrophic flagellates account for up to half of pigmented biomass. Chl-a maxima develop at the	(Aquilina et al., 2010; Chen et al., 2017; Dale et al., 2008b; Havskum and Riemann, 1996; Jensen et al., 1990; Lomstein et al., 1990; Thamdrup et al., 1994;

https://doi.org/10.5194/bg-2020-435
Preprint. Discussion started: 6 January 2021

												pycnocline. Spring phytoplankton blooms dominated by diatoms.	Thingstad et al., 1996)
E	Arkona Basin 348GC 351GC	54.80 N 13.78 E	Temperate (Cfb)	Shelf 43	$7.4 \cdot 10^{-3}$ 5.0	Sub-oxic	EUR1	5.0 N/A	N/A N/A	Mostly terrestrial Fluvial	Bioturbated	Phytoplankton community shows a yearly variation. Spring blooms are mainly dominated by diatoms and dinoflagellates. A late cyanobacteria bloom occurs in the end of summer. Long-term decrease in water transparency associated to eutrophication, which favours phytoplankton growth occurs during spring blooms.	(Fleming and Kaitala, 2006; Fleming-Lehtinen and Laamanen, 2012; Mogollón et al., 2012; Zettler et al., 2007)
F	Helgoland Mud Area, North Sea HE443-010	54.08 N 7.97 E	Temperate (Cfb)	Shelf 29	$1.3 \cdot 10^{0}$ 10.0	Anoxic	EUR1	1.1 N/A	−174 – 195 N/A	Marine in the uppermost sediments and largely terrestrial at depth Marine PP and fluvial	Non-Bioturbated	Diatoms spring blooms. Flagellates growth is restricted to summer months, associated with higher temperatures and nutrient regeneration. Low phytoplankton biomass during winter months. Haptophytes can represent a large contribution to phytoplankton community, although the timing and intensity of blooms vary in a less predictive way.	(Hebbeln et al., 2003; Henkel and Kulkarni, 2015; Hickel et al., 1992; Riebesell, 1993; Wiltshire and Manly, 2004)
G	Skagerrak S10 807GC 808GC	57.92 N 9.75 E	Temperate (Cfb)	Shelf 86	$5.0 \cdot 10^{-1}$ 8.7	Oxic	EUR1	1.3 0.6 – 0.7	N/A N/A	Largely terrestrial Fluvial and marine PP	Bioturbated	Sub-surface Chl-a maxima below pycnocline, which are photosynthetically active and result of distinct bloom events. Diatoms dominant during	(Aquilina et al., 2010; Canfield et al., 1993; Dahl and Johannessen, 1998; Dale et al., 2008a; Karlson et
H	Skagerrak S11	57.95 N	Temperate (Cfb)	Shelf 150	$5.0 \cdot 10^{-1}$ 9.8	Oxic	EUR1	0.5	N/A N/A	Largely terrestrial	Bioturbated		

https://doi.org/10.5194/bg-2020-435
Preprint. Discussion started: 6 January 2021

	816GC 836GC	9.70 E						0.6 – 0.7		Fluvial and marine PP		spring, whereas dinoflagellates are predominant during summer. Prysmnesiophyceae account for half of nanophytoplankton. Cyanobacteria abundance is high in the central basin during summer. Nevertheless, spring and summer blooms are not characteristic, instead short-term and inter-annual variability in Chl-a and phytoplankton community are common.	al., 1996; Knab et al., 2008; Mayer, 1994b; Richardson et al., 2003; Trimmer et al., 2013)
I	Skagerrak S13 786GC 789GC	58.05 N 9.60 E	Temperate (Cfb)	Slope 386	$5.0 \cdot 10^{-1}$ 4.5	Oxic	EUR1	1.8 0.6 – 0.7	N/A N/A	Largely terrestrial Fluvial and marine PP	Bioturbated		
J	Arabian Sea (Core of OMZ) GeoB 12312	24.88 N 63.02 E	Arid (BWh)	Slope 654	$5.0 \cdot 10^{-2}$ 11.6	Anoxic	WARAB	0.92 1.1 – 2.3	N/A 0.800 – 0.920	Largely marine Marine PP	Non-Bioturbated	Monsoon regime drives hydrology and has a strong impact on primary productivity. The SW monsoon triggers upwellings, whereas the NE monsoon causes cooling of surface waters and deepening of the mixed layer. Cyanobacteria dominates oligotrophic, warm upper waters and during NE monsoon. In subsurface and during SW monsoon eukaryotic phytoplankton are the dominant group and represents 50-80% of carbon biomass. Among them, diatoms dominate coastal upwellings and are gradually replaced offshore by haptophytes.	(Bard et al., 2013; Barlow et al., 1999; Cowie, 2005; Keil and Cowie, 1999; Koho et al., 2013; Latasa and Bidigare, 1998; Luff et al., 2000; Rixen et al., 2019; Shalapyonok et al., 2001; Vandewiele et al., 2009)
K	Arabian Sea (OMZ transition) GeoB 12309	24.81 N 62.99 E	Arid (BWh)	Slope 957	$5.0 \cdot 10^{-2}$ 9.6	Anoxic	WARAB	0.89 1.1 – 2.3	N/A 0.800 – 0.920	Largely marine Marine PP	Non-Bioturbated		
L	Arabian Sea (Below OMZ) GeoB 12308	24.71 N 62.99 E	Arid (BWh)	Slope 1,586	$5.0 \cdot 10^{-2}$ 5.1	Oxic	WARAB	0.87 0.4 – 1.1	N/A 0.800 – 0.920	Largely marine Marine PP	Bioturbated		

https://doi.org/10.5194/bg-2020-435
Preprint. Discussion started: 6 January 2021

M	Bering Sea SO202-22	54.57 N 168.81 W	Temperate (Cfb) Snow (Dfc) Polar (ET/EF)	Slope 1,476	$1.6 \cdot 10^{-3}$ 2.0	Oxic	NWPAC	1.3 N/A	−143 0.857	Largely marine Marine PP	Bioturbated	Spring blooms triggered by ice melting and autumn blooms supported by remineralization and nutrient upwelling. In the absence of sea ice, spring blooms are delayed until thermal stratification is established by surface heating. Coccolithophores form large blooms during calm conditions with variable extents and occurrence areas. Overall, community composition is dominated by diatoms with small contribution of pico- and nanophytoplankton groups.	(Coyle et al., 2008; Gersonde, 2009; Odate, 1996; Stabeno and Hunt, 2002; Stockwell et al., 2001)
N	Argentine Basin GeoB 13863	39.31 S 53.95 W	Temperate (Cfa/Cfb)	Slope 3,687	$8.0 \cdot 10^{-3}$ 3.5	Oxic	RIOPLATA	1.0 N/A	N/A 0.777	Mixed marine and terrestrial Lateral transport across the shelf to slope	Bioturbated	Complex hydrology and water masses dynamics. Enhanced productivity at oceanographic fronts and Sub-Antarctic water upwellings. Haptophytes are the dominant group, whereas diatoms occur in low abundance. Other groups include pico-cyanobacteria, picoplanktonic coccoids, and flagellates. Coccolithophore blooms are common at the	(Benthien and Müller, 2000; Calliari et al., 2009, 2009; Carreto et al., 2003; Gayoso, 1995; Henkel et al., 2011; Mollenhauer et al., 2006; Peterson, 1992)

https://doi.org/10.5194/bg-2020-435
Preprint. Discussion started: 6 January 2021

		shelf-break, where strong mixing and nutrient renovation occur.

https://doi.org/10.5194/bg-2020-435
Preprint. Discussion started: 6 January 2021

990 **Table 2. Global transport and reaction parameters governing organic matter heterotrophic degradation in marine sediments.**

Parameter		Unit	Value	Reference
		Transport parameters		
Length of model domain	L	cm	1000*	This study
Bioirrigation coefficient	a_0	y^{-1}	10	Thullner et al. (2009)
Bioirrigation attenuation depth	x_{irri}	cm	3.5	Thullner et al. (2009)
Oxygen molecular diffusion coefficient	D_{O_2}	$cm^2\ y^{-1}$	380.44	Van Cappellen and Wang (1996)
Nitrate molecular diffusion coefficient	$D_{NO_3^-}$	$cm^2\ y^{-1}$	394.58	Van Cappellen and Wang (1996)
Sulfate molecular diffusion coefficient	$D_{SO_4^{2-}}$	$cm^2\ y^{-1}$	173.92	Van Cappellen and Wang (1996)
Ammonium molecular diffusion coefficient	$D_{NH_4^+}$	$cm^2\ y^{-1}$	395.87	Van Cappellen and Wang (1996)
Hydrogen sulfide molecular diffusion coefficient	D_{H_2S}	$cm^2\ y^{-1}$	331.61	Van Cappellen and Wang (1996)
Methane molecular diffusion coefficient	$D_{CH_{4(g)}}$	$cm^2\ y^{-1}$	263.93	Van Cappellen and Wang (1996)
		Reaction parameters		
Stoichiometry constants	$x/y/z$	–	106/16/1	Redfield (1934)
Organic matter reactivity scaling parameter	v	–	variable	Boudreau and Ruddick (1991)
Organic matter reactivity shaping parameter	α	y	variable	Boudreau and Ruddick (1991)
Organic matter reactivity – multi-G	k_{MG}	y^{-1}	$10^{-15} - 10^{-\log(a)+2}$	Jørgensen (1978)
Organic matter age	age	y	variable	Mogollón et al. (2012)
Oxygen half saturation constant	K_{O_2}	M	$8.0 \cdot 10^{-9}$	Van Cappellen and Wang (1996)
Nitrate half saturation constant	$K_{NO_3^-}$	M	$5.0 \cdot 10^{-9}$	Van Cappellen and Wang (1996)
Sulfate half saturation constant	$K_{SO_4^{2-}}$	M	$1.0 \cdot 10^{-7}$	Van Cappellen and Wang (1996)
Ammonium oxidation (oxygen) rate constant	k_5	$M^{-1}\ y^{-1}$	$1.0 \cdot 10^{7}$	Dale et al. (2011)
Sulfide oxidation (oxygen) rate constant	k_6	$M^{-1}\ y^{-1}$	$1.0 \cdot 10^{9}$	Dale et al. (2011)
Methane oxidation (sulfate – AOM) rate constant	k_7	$M^{-1}\ y^{-1}$	$5.0 \cdot 10^{6}$	Dale et al. (2011)
Methane oxidation (oxygen) rate constant	k_8	$M^{-1}\ y^{-1}$	$1.0 \cdot 10^{13}$	Dale et al. (2011)

995

https://doi.org/10.5194/bg-2020-435
Preprint. Discussion started: 6 January 2021

Biogeosciences Discussions Open Access EGU

Table 3. Site-specific transport parameters and upper boundary conditions implemented in the Reaction-Transport Model.

	Site-specific transport parameters							*Site-specific upper boundary conditions*					
Location	**Porosity**	**Bioturbation coefficient**	**Bioturbation depth**	**Sedimentation rate**	**Temperature**	**Salinity**	**Depth**	**Organic carbon**	**Oxygen**	**Nitrate**	**Sulfate**	**Methane**	**Sulfides**
	φ	D_{bio}	z_{bio}	ω	T	S	h	POC	O_2	NO_3^-	SO_4^{2-}	CH_4	HS^-
	-	$cm^2\ y^{-1}$	cm	$cm\ y^{-1}$	°C	-	m	wt%	µM	µM	mM	µM	mM
A	0.70	29.8	9	$4.3 \cdot 10^{-1}$	18.0	35	8	3.0	0	30	23	0	0
B	0.80	0.50	10	$1.0 \cdot 10^{1}$	16.8	35	18	2.0	245	25	28	0	0
C	0.83	10.0	10	$5.0 \cdot 10^{-1}$	14.4	35	75	1.3	225	25	29	0	0
D	0.86	0	0	$3.2 \cdot 10^{-1}$	12.0	35	15	3.5	0	0	20	0	0
E	0.86	0	0	$7.4 \cdot 10^{-3}$	5.0	35	43	5.0	0	0	6	0	0
F	0.70	0	0	$1.3 \cdot 10^{0}$	10.0	35	30	1.1	0	0	26	0	0
G	0.44	27.8	10	$5.0 \cdot 10^{-1}$	8.7	35	86	1.3	250	25	29	0	0
H	0.47	26.3	10	$5.0 \cdot 10^{-1}$	9.8	35	147	0.5	250	25	29	0	0
I	0.50	0	0	$5.0 \cdot 10^{-1}$	4,5	35	386	1.8	0	0	22	0	0
J	0.60	0	0	$5.0 \cdot 10^{-2}$	11.6	35	632	5.0	0	0	25	0	0
K	0.60	0	0	$5.0 \cdot 10^{-2}$	9.6	35	930	4.4	0	0	28	0	0
L	0.70	7.3	10	$5.0 \cdot 10^{-2}$	5.1	35	1,552	4.3	250	25	29	0	0
M	0.60	7.8	10	$1.6 \cdot 10^{-3}$	2.0	35	1,469	1.3	250	25	28	0	0
N	0.70	1.0	10	$8.0 \cdot 10^{-3}$	3.5	35	3,687	1.0	250	25	28	0	0

1000

https://doi.org/10.5194/bg-2020-435
Preprint. Discussion started: 6 January 2021

Biogeosciences Discussions Open Access EGU

1005 **Table 4. Benthic organic matter dynamics derived from the coupled model-data assessments across the contrasting depositional settings.**

		OM reactivity			*OM degradation dynamics*				*Benthic-pelagic fluxes*				
	Site	a	v	$k(0)$	F_{OM}	$\sum R_C$	$\sum AOM$	$SMTZ$	$\sum J_{O2}$	$\sum J_{NO3}$	$\sum J_{SO4}$	$\sum J_{NH4}$	$\sum J_{PO4}$
		y	-	y^{-1}	mol C cm^{-2} y^{-1}	mol C cm^{-2} y^{-1}	mol C cm^{-2} y^{-1}	cmbsf	µmol O_2 cm^{-2} y^{-1}	µmol NO_3^- cm^{-2} y^{-1}	µmol SO_4^{2-} cm^{-2} y^{-1}	µmol NH_4^+ cm^{-2} y^{-1}	µmol PO_4^{3-} cm^{-2} y^{-1}
A	Severn estuary	$5.0 \cdot 10^{1}$	0.100	$2.0 \cdot 10^{-3}$	$1.55 \cdot 10^{-3}$	$9.89 \cdot 10^{-4}$	$9.2 \cdot 10^{-5}$	35	n.d	−145	−178	39.9	0.93
B	Rhone proximal	$3.0 \cdot 10^{0}$	0.125	$4.2 \cdot 10^{-2}$	$2.04 \cdot 10^{-2}$	$1.50 \cdot 10^{-2}$	$1.6 \cdot 10^{-4}$	24	−1,649	−132	−612	110	0.79
C	Rhone shelf	$1.0 \cdot 10^{2}$	0.125	$1.3 \cdot 10^{-3}$	$5.76 \cdot 10^{-4}$	$4.19 \cdot 10^{-4}$	$4.8 \cdot 10^{-6}$	537	−81.2	−1.3	−30.3	9.8	0.03
D	Aarhus Bay	$1.0 \cdot 10^{0}$	0.060	$6.0 \cdot 10^{-2}$	$1.05 \cdot 10^{-3}$	$8.55 \cdot 10^{-4}$	$1.2 \cdot 10^{-5}$	185	n.d	n.d	−462	278	5.6
E	Arkona Basin	$1.0 \cdot 10^{0}$	0.155	$1.6 \cdot 10^{-1}$	$7.42 \cdot 10^{-4}$	$7.17 \cdot 10^{-4}$	$8.8 \cdot 10^{-6}$	68	n.d	n.d	−715	467	9.1
F	Helgoland Mud Area, North Sea	$3.0 \cdot 10^{1}$	0.125	$4.2 \cdot 10^{-3}$	$1.59 \cdot 10^{-3}$	$1.00 \cdot 10^{-3}$	$5.0 \cdot 10^{-5}$	58	n.d	n.d	−98.7	24.1	0.22
G	Skagerrak S10	$1.8 \cdot 10^{3}$	0.100	$5.6 \cdot 10^{-5}$	$8.27 \cdot 10^{-4}$	$1.00 \cdot 10^{-4}$	$1.7 \cdot 10^{-5}$	145	−36.7	−0.77	−26.2	4.1	0
H	Skagerrak S11	$1.0 \cdot 10^{1}$	0.130	$1.3 \cdot 10^{-2}$	$4.10 \cdot 10^{-4}$	$2.74 \cdot 10^{-4}$	$3.2 \cdot 10^{-5}$	68	−472	−2.7	−108	65.5	1.4
I	Skagerrak S13	$3.5 \cdot 10^{3}$	0.110	$3.1 \cdot 10^{-5}$	$9.9 \cdot 10^{-4}$	$9.04 \cdot 10^{-5}$	$1.8 \cdot 10^{-5}$	98	n.d	n.d	−16.8	1.9	0
J	Arabian Sea OMZ core	$1.0 \cdot 10^{0}$	0.250	$2.5 \cdot 10^{-1}$	$7.51 \cdot 10^{-4}$	$7.30 \cdot 10^{-4}$	$7.8 \cdot 10^{-6}$	195	n.d	n.d	−2,816	1,824	36.9
K	Arabian Sea OMZ transition	$1.0 \cdot 10^{1}$	0.390	$3.9 \cdot 10^{-2}$	$4.88 \cdot 10^{-4}$	$4.78 \cdot 10^{-4}$	$5.1 \cdot 10^{-6}$	255	n.d	n.d	−968	611	12.9
L	Arabian Sea below OMZ	$1.0 \cdot 10^{1}$	0.330	$3.3 \cdot 10^{-2}$	$1.31 \cdot 10^{-3}$	$1.30 \cdot 10^{-3}$	$2.4 \cdot 10^{-6}$	410	−1,021	−96.8	−642	439	10.8
M	Bering Sea	$5.0 \cdot 10^{3}$	0.270	$5.4 \cdot 10^{-5}$	$3.72 \cdot 10^{-5}$	$2.82 \cdot 10^{-5}$	$1.4 \cdot 10^{-6}$	705	−17.3	−0.42	−5.1	2.7	0.03
N	Argentine Basin	$2.0 \cdot 10^{3}$	0.125	$6.3 \cdot 10^{-5}$	$6.0 \cdot 10^{-5}$	$3.06 \cdot 10^{-5}$	$2.3 \cdot 10^{-6}$	527	−17.7	−0.36	−5.0	2.5	0.01

n.d.: not determined (oxygen and nitrate benthic fluxes not determined for locations where SWI concentrations of those TEA were assumed to be zero).

https://doi.org/10.5194/bg-2020-435
Preprint. Discussion started: 6 January 2021

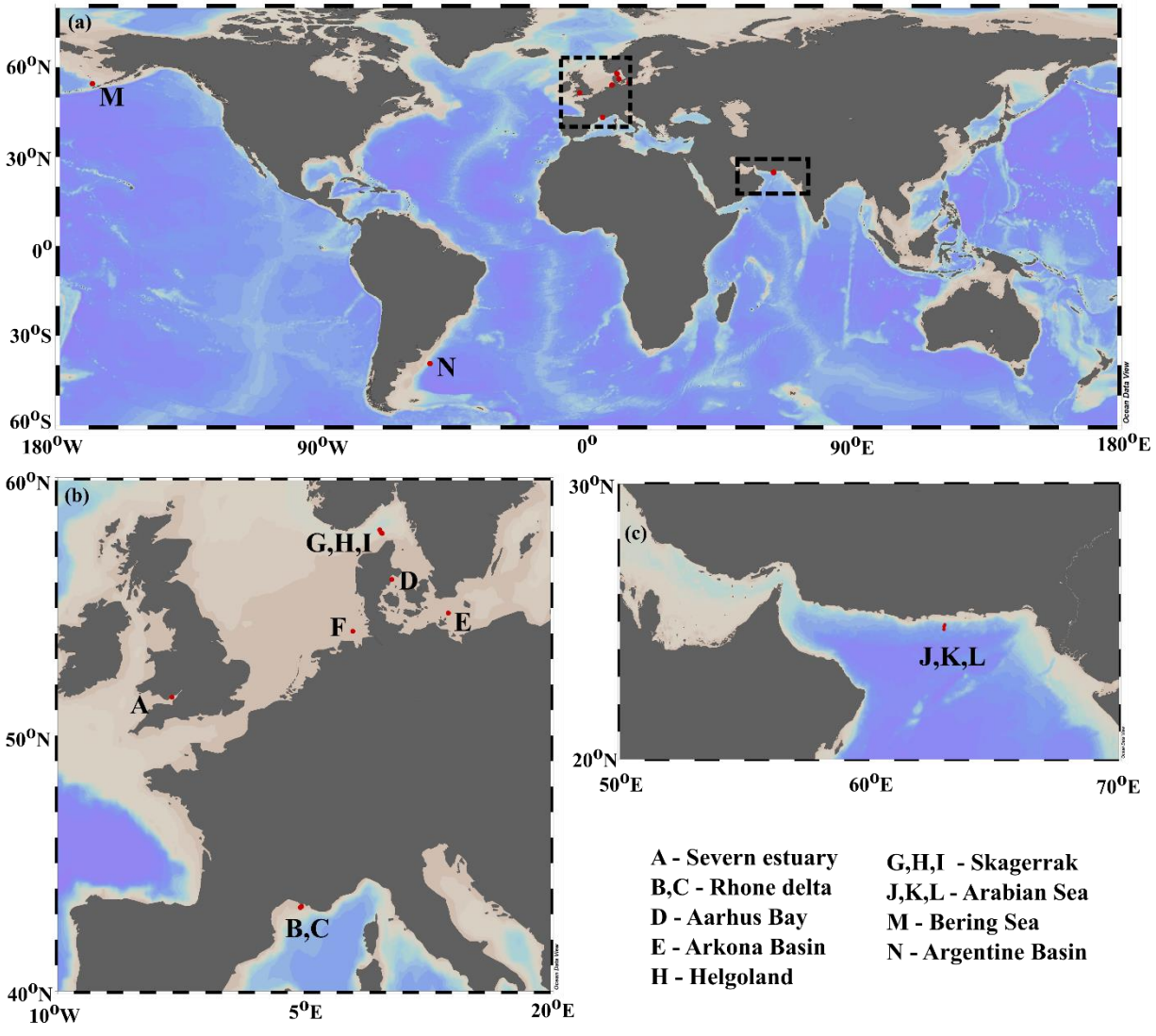

1010 **Figure 1. Depositional environment geographic locations. (a) Global scale; (b) European margin; (c) Arabian Sea region. Map produced with Ocean Data View** (Schlitzer, 2019)**.**

https://doi.org/10.5194/bg-2020-435
Preprint. Discussion started: 6 January 2021

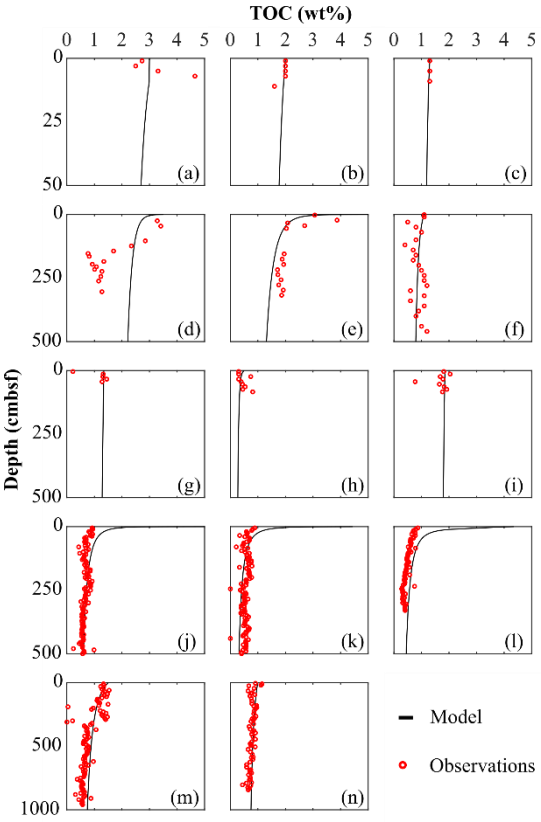

Figure 2. Total organic carbon data-model best fit: (a) Severn estuary; (b) Rhone pro-delta; (c) Rhone shelf; (d) Aarhus Bay; (e) Arkona Basin; (f) Helgoland Mud Area, North Sea; (g) Skagerrak – S10; (h) Skagerrak – S11; (i) Skagerrak – S13; (j) Arabian Sea – OMZ core; (k) Arabian Sea – OMZ transition; (l) Arabian Sea – below OMZ; (m) Bering Sea; (n) Argentine Basin.

https://doi.org/10.5194/bg-2020-435
Preprint. Discussion started: 6 January 2021

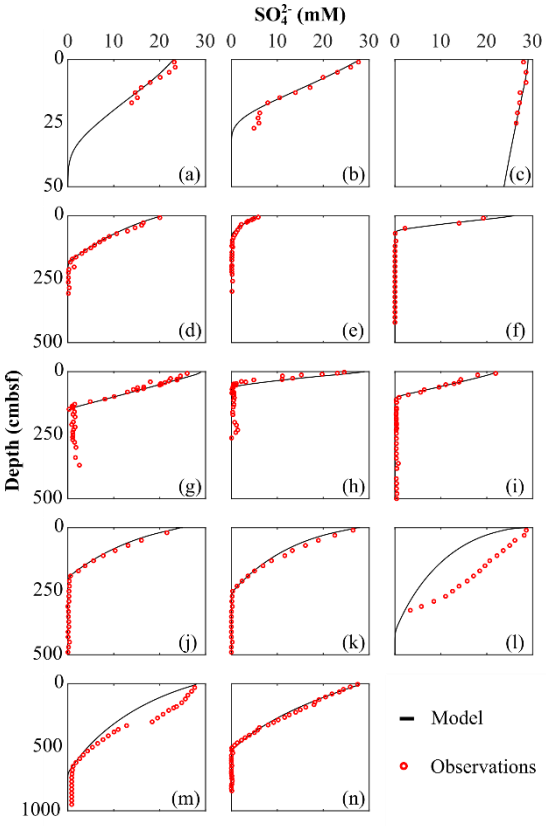

Figure 3. Sulfate data-model best-fit: (a) Severn estuary; (b) Rhone pro-delta; (c) Rhone shelf; (d) Aarhus Bay; (e) Arkona Basin; (f) Helgoland Mud Area, North Sea; (g) Skagerrak – S10; (h) Skagerrak – S11; (i) Skagerrak – S13; (j) Arabian Sea – OMZ core; (k) Arabian Sea – OMZ transition; (l) Arabian Sea – below OMZ; (m) Bering Sea; (n) Argentine Basin.

https://doi.org/10.5194/bg-2020-435
Preprint. Discussion started: 6 January 2021

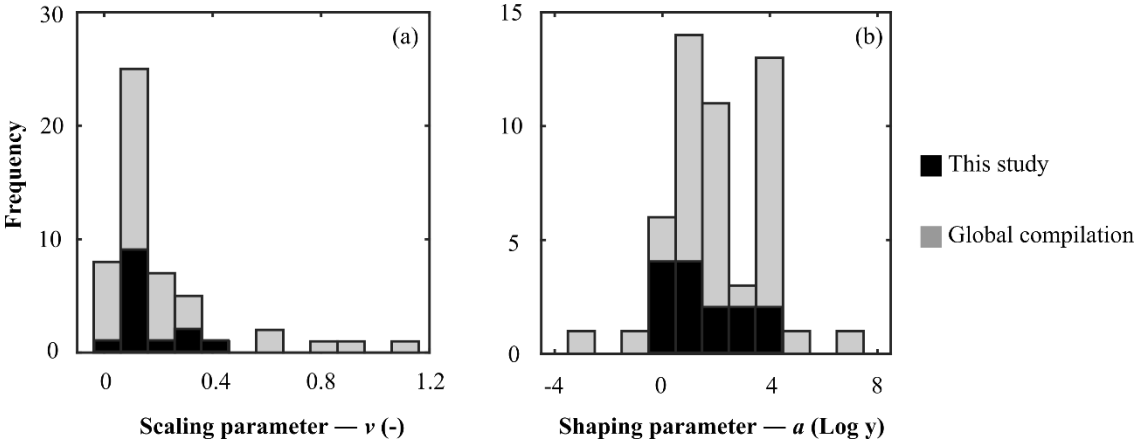

Figure 4. Frequency histogram of organic matter reactivity parameters distribution in a global scale: (a) scaling parameter – v; (b) shaping parameter – a.

1030

https://doi.org/10.5194/bg-2020-435
Preprint. Discussion started: 6 January 2021

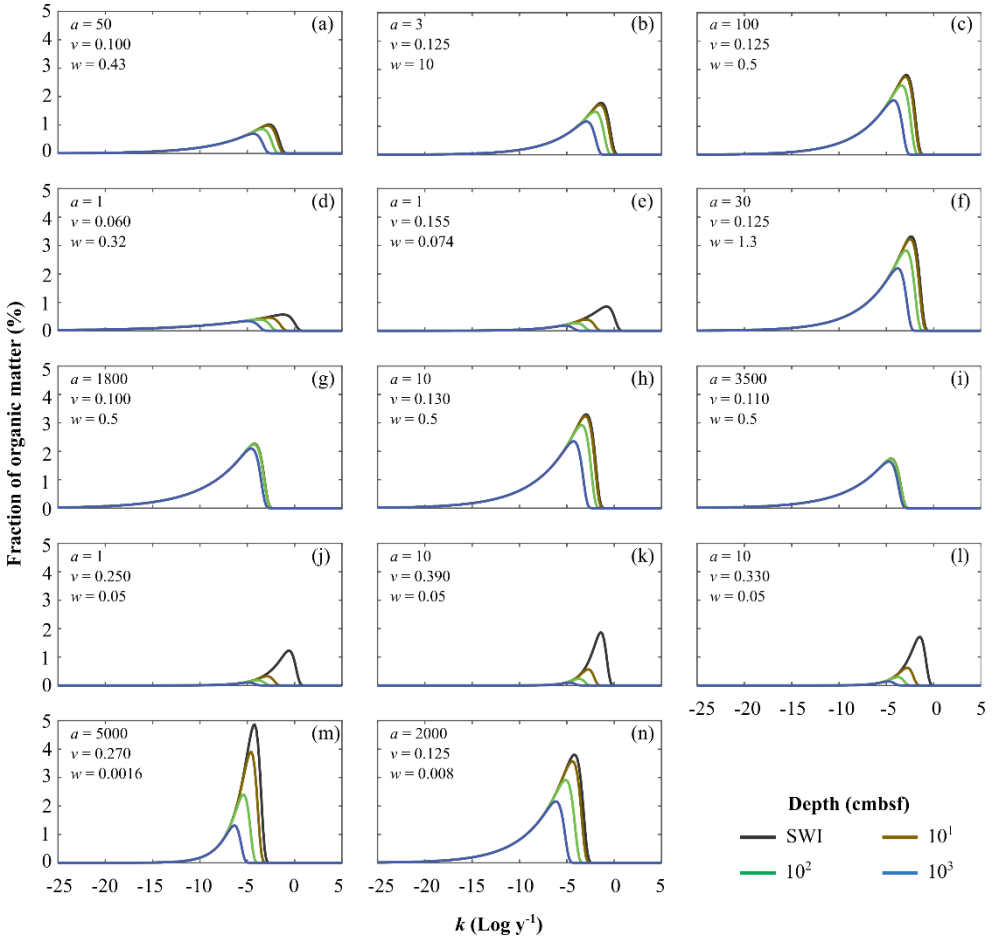

Figure 5. Apparent organic matter reactivity *k* initial probability distributions and downcore evolution as function of burial depths: (a) Severn estuary; (b) Rhone pro-delta; (c) Rhone shelf; (d) Aarhus Bay; (e) Arkona Basin; (f) Helgoland Mud Area, North Sea; (g) Skagerrak – S10; (h) Skagerrak – S11; (i) Skagerrak – S13; (j) Arabian Sea – OMZ core; (k) Arabian Sea – OMZ transition; (l) Arabian Sea – below OMZ; (m) Bering Sea; (n) Argentine Basin.

https://doi.org/10.5194/bg-2020-435
Preprint. Discussion started: 6 January 2021

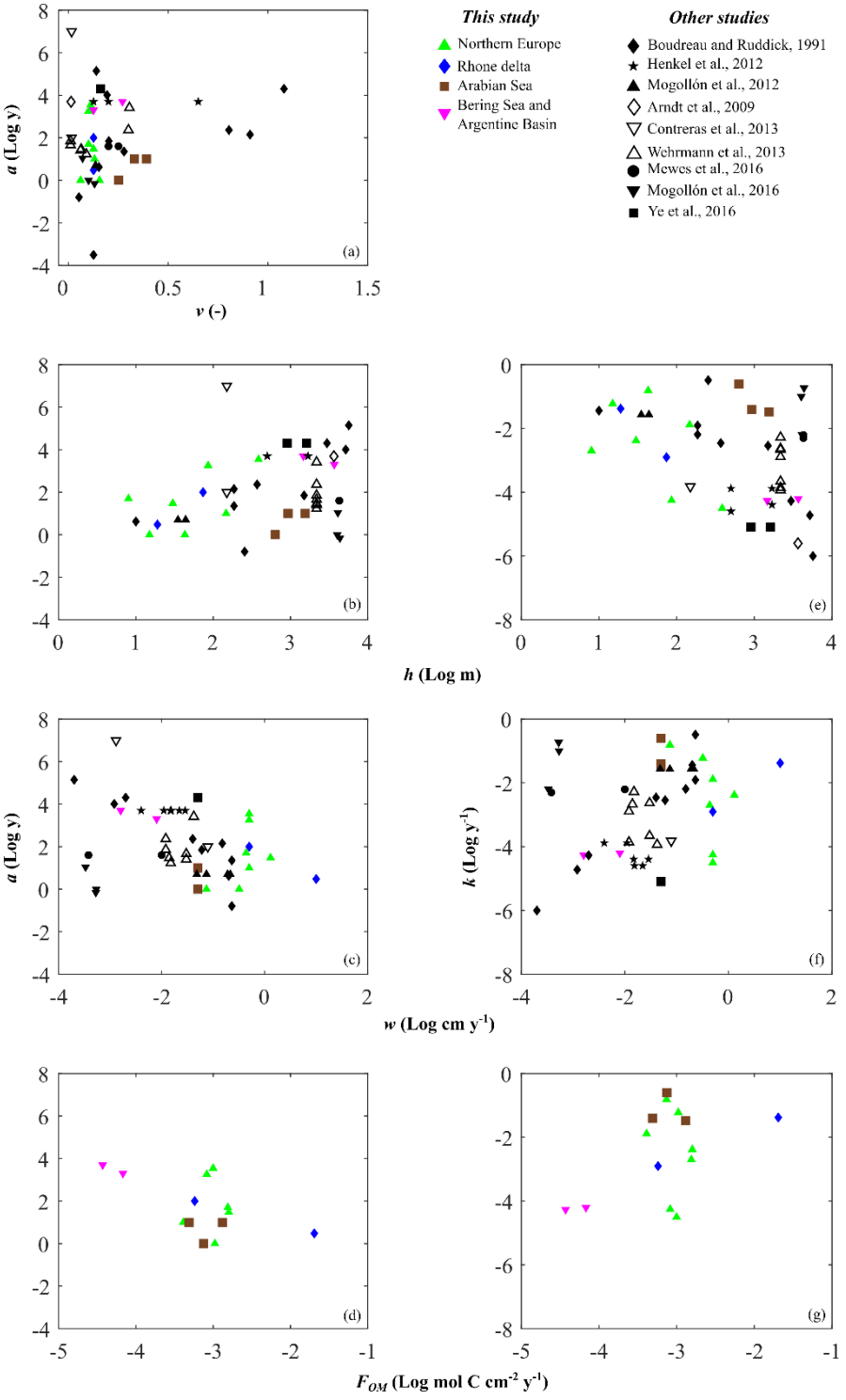

Figure 6. Depositional environment controls on organic matter reactivity parameters a (a – d) and k (e – g): (a) v vs. a; (b, e) water depth h; (c, f) sedimentation rate ω; (d, g) organic matter fluxes F_{OM}.

https://doi.org/10.5194/bg-2020-435
Preprint. Discussion started: 6 January 2021

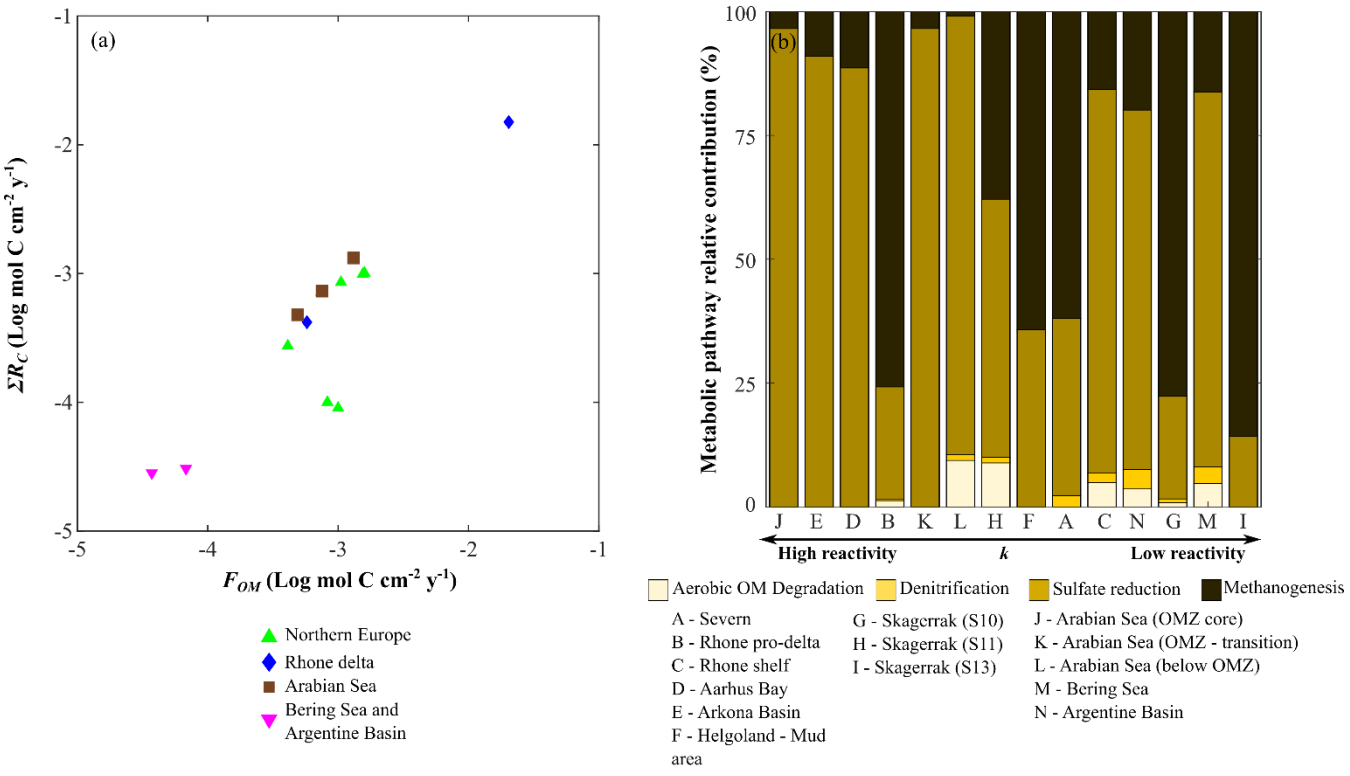

Figure 7. Benthic organic matter degradation dynamics. (a) organic matter fluxes vs. depth-integrated organic matter degradation rates; (b) Relative contribution of each metabolic pathway to heterotrophic organic matter degradation.

1045

https://doi.org/10.5194/bg-2020-435
Preprint. Discussion started: 6 January 2021

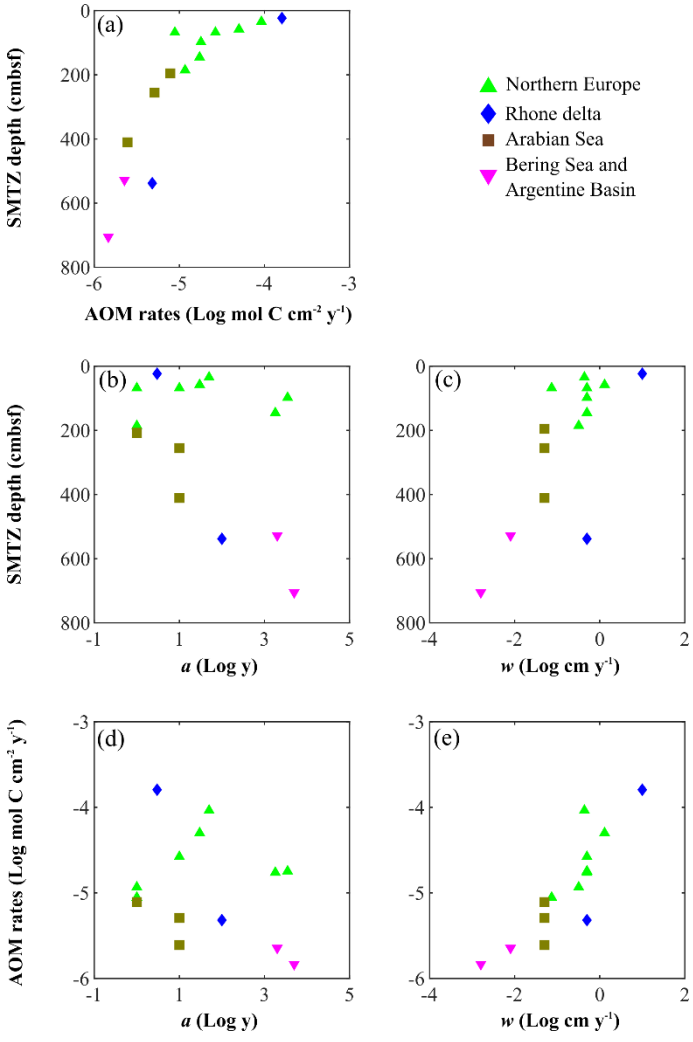

Figure 8. Anaerobic oxidation of methane (AOM) patterns as a function of apparent organic matter reactivity and depositional rates. (a) AOM rates *vs.* SMTZ depth; SMTZ depths *vs.* (b) reactivity parameter *a* and (c) sedimentation rates *ω*; AOM rates *vs.* (d) reactivity parameter *a* and (e) sedimentation rates *ω*.

https://doi.org/10.5194/bg-2020-435
Preprint. Discussion started: 6 January 2021

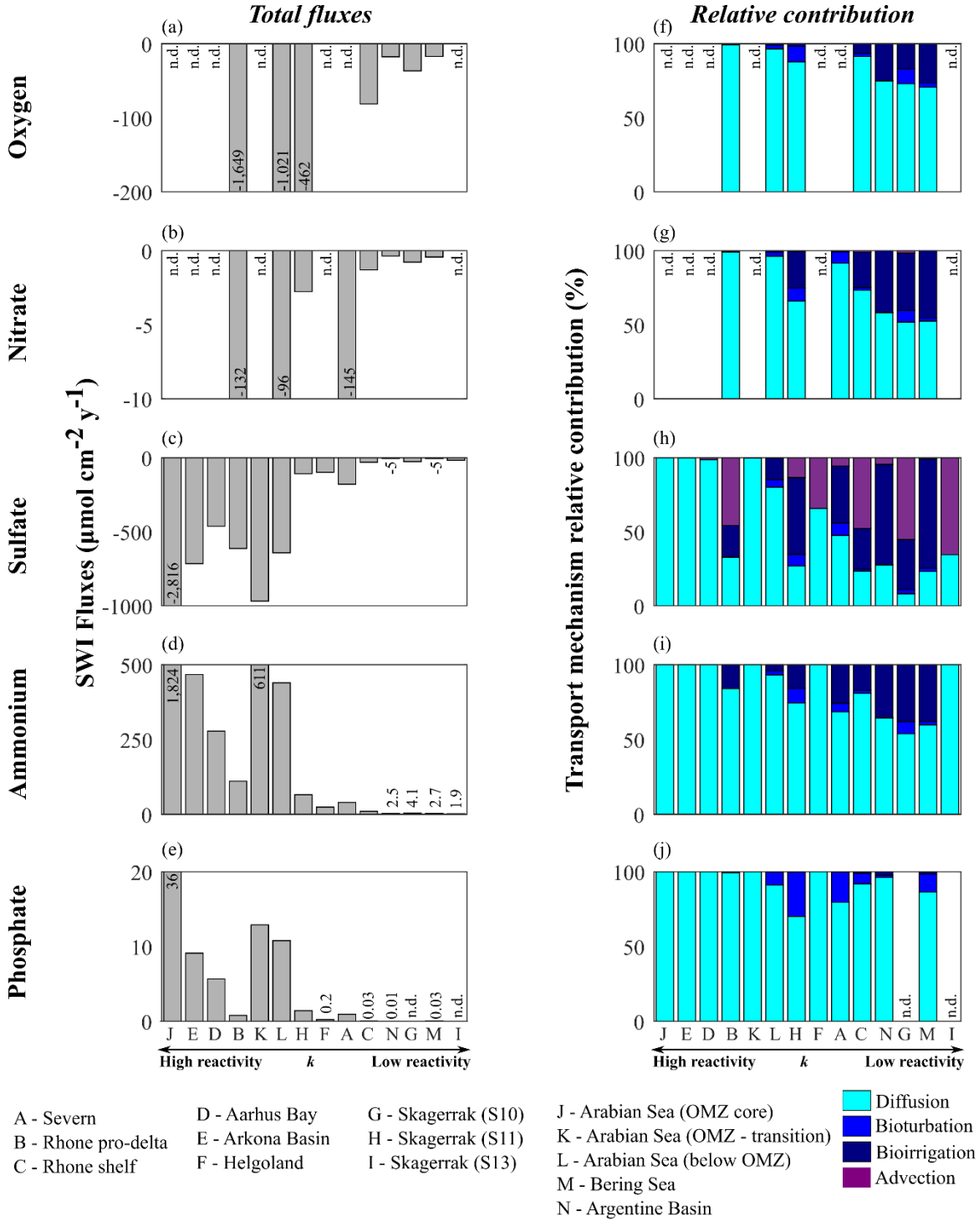

Figure 9. Benthic fluxes of dissolved species (a–e) and transport mechanism relative contributions (f–j): (a,f) oxygen; (b,g) nitrate; (c,h) sulfate; (d,i) ammonium; (e,j) phosphate.

https://doi.org/10.5194/bg-2020-435
Preprint. Discussion started: 6 January 2021

References

Aguilera, D. R., Jourabchi, P., Spiteri, C. and Regnier, P.: A knowledge-based reactive transport approach for the simulation of biogeochemical dynamics in Earth systems, Geochem. Geophys. Geosystems, 6(7), 1–18, doi:10.1029/2004GC000899, 2005.

Ait Ballagh, F. E., Rabouille, C., Andrieux-Loyer, F., Soetaert, K., Elkalay, K. and Khalil, K.: Spatio-temporal dynamics of sedimentary phosphorus along two temperate eutrophic estuaries: A data-modelling approach, Cont. Shelf Res., 193, 104037, doi:10.1016/j.csr.2019.104037, 2020.

Aller, R. C.: Diagenetic Processes Near the Sediment-Water Interface of Long Island Sound. I., in Advances in Geophysics, vol. 22, pp. 237–350, Elsevier., 1980.

Aller, R. C.: Bioturbation and remineralization of sedimentary organic matter: effects of redox oscillation, Chem. Geol., 114(3–4), 331–345, doi:10.1016/0009-2541(94)90062-0, 1994.

Aller, R. C. and Aller, J. Y.: The effect of biogenic irrigation intensity and solute exchange on diagenetic reaction rates in marine sediments, J. Mar. Res., 56(4), 905–936, doi:10.1357/002224098321667413, 1998.

Antonelli, C., Eyrolle, F., Rolland, B., Provansal, M. and Sabatier, F.: Suspended sediment and 137Cs fluxes during the exceptional December 2003 flood in the Rhone River, southeast France, Geomorphology, 95(3–4), 350–360, doi:10.1016/j.geomorph.2007.06.007, 2008.

Aquilina, A., Knab, N. J., Knittel, K., Kaur, G., Geissler, A., Kelly, S. P., Fossing, H., Boot, C. S., Parkes, R. J., Mills, R. A., Boetius, A., Lloyd, J. R. and Pancost, R. D.: Biomarker indicators for anaerobic oxidizers of methane in brackish-marine sediments with diffusive methane fluxes, Org. Geochem., 41(4), 414–426, doi:10.1016/j.orggeochem.2009.09.009, 2010.

Aris, R.: Prolegomena to the rational analysis of systems of chemical reactions II. Some addenda, Arch. Ration. Mech. Anal., 27(5), 356–364, doi:10.1007/BF00251438, 1968.

Arndt, S., Hetzel, A. and Brumsack, H.-J.: Evolution of organic matter degradation in Cretaceous black shales inferred from authigenic barite: A reaction-transport model, Geochim. Cosmochim. Acta, 73(7), 2000–2022, doi:10.1016/j.gca.2009.01.018, 2009.

Arndt, S., Jørgensen, B. B., LaRowe, D. E., Middelburg, J. J., Pancost, R. D. and Regnier, P.: Quantifying the degradation of organic matter in marine sediments: A review and synthesis, Earth-Sci. Rev., 123, 53–86, doi:laro, 2013.

Arning, E. T., van Berk, W. and Schulz, H.-M.: Fate and behaviour of marine organic matter during burial of anoxic sediments: Testing CH_2O as generalized input parameter in reaction transport models, Mar. Chem., 178, 8–21, doi:10.1016/j.marchem.2015.12.002, 2016.

Aromokeye, D. A., Oni, O. E., Tebben, J., Yin, X., Richter-Heitmann, T., Wendt, J., Nimzyk, R., Littmann, S., Tienken, D., Kulkarni, A., Henkel, S., Hinrichs, K.-U., Elvert, M., Harder, T., Kasten, S., Michael, W. and Friedrich, M. W.: Crystalline iron oxides stimulate methanogenic benzoate degradation in marine sediment- derived enrichment cultures, The ISME Journal., Accepted.

Aromokeye, D. A., Oni, O. E., Tebben, J., Yin, X., Richter-Heitmann, T., Wendt, J., Nimzyk, R., Littmann, S., Tienken, D., Kulkarni, A. C., Henkel, S., Hinrichs, K.-U., Elvert, M., Harder, T., Kasten, S. and Friedrich, M. W.: Crystalline iron oxides stimulate methanogenic benzoate degradation in marine sediment-derived enrichment cultures, ISME J., doi:10.1038/s41396-020-00824-7, 2020.

Bach, L. T., Stange, P., Taucher, J., Achterberg, E. P., Algueró-Muñiz, M., Horn, H., Esposito, M. and Riebesell, U.: The Influence of Plankton Community Structure on Sinking Velocity and Remineralization Rate of Marine Aggregates, Glob. Biogeochem. Cycles, 33(8), 971–994, doi:10.1029/2019GB006256, 2019.

Bahr, A., Pape, T., Bohrmann, G., Mazzini, A., Haeckel, M., Reitz, A. and Ivanov, M.: Authigenic carbonate precipitates from the NE Black Sea: a mineralogical, geochemical, and lipid biomarker study, Int. J. Earth Sci., 98(3), 677–695, doi:10.1007/s00531-007-0264-1, 2009.

Bard, E., Ménot, G., Rostek, F., Licari, L., Böning, P., Edwards, R. L., Cheng, H., Wang, Y. and Heaton, T. J.: Radiocarbon Calibration/Comparison Records Based on Marine Sediments from the Pakistan and Iberian Margins, Radiocarbon, 55(4), 1999–2019, doi:10.2458/azu_js_rc.55.17114, 2013.

Barlow, R. G., Mantoura, R. F. C. and Cummings, D. G.: Monsoonal influence on the distribution of phytoplankton pigments in the Arabian Sea, Deep Sea Res. Part II Top. Stud. Oceanogr., 46(3–4), 677–699, doi:10.1016/S0967-0645(98)00123-4, 1999.

Beckler, J. S., Kiriazis, N., Rabouille, C., Stewart, F. J. and Taillefert, M.: Importance of microbial iron reduction in deep sediments of river-dominated continental-margins, Mar. Chem., 178, 22–34, doi:10.1016/j.marchem.2015.12.003, 2016.

Benthien, A. and Müller, P. J.: Anomalously low alkenone temperatures caused by lateral particle and sediment transport in the Malvinas Current region, western Argentine Basin, Deep Sea Res. Part Oceanogr. Res. Pap., 47(12), 2369–2393, doi:10.1016/S0967-0637(00)00030-3, 2000.

Berner, R. A.: Early diagenesis: a theoretical approach, Princeton University Press, Princeton, N.J., 1980.

Berner, R. A.: The long-term carbon cycle, fossil fuels and atmospheric composition, Nature, 426(6964), 323–326, doi:10.1038/nature02131, 2003.

Bianchi, T. S., Cui, X., Blair, N. E., Burdige, D. J., Eglinton, T. I. and Galy, V.: Centers of organic carbon burial and oxidation at the land-ocean interface, Org. Geochem., 115, 138–155, doi:10.1016/j.orggeochem.2017.09.008, 2018.

Bogus, K. A., Zonneveld, K. A. F., Fischer, D., Kasten, S., Bohrmann, G. and Versteegh, G. J. M.: The effect of meter-scale lateral oxygen gradients at the sediment-water interface on selected organic matter based alteration, productivity and temperature proxies, Biogeosciences, 9(4), 1553–1570, doi:10.5194/bg-9-1553-2012, 2012.

Bohrmann, G. and cruise participants: Documentation of sediment core GeoB12308-5, PANGAEA, doi:10.1594/PANGAEA.737529, 2010a.

Bohrmann, G. and cruise participants: Documentation of sediment core GeoB12309-3, PANGAEA, doi:10.1594/PANGAEA.737530, 2010b.

Bohrmann, G. and cruise participants: Documentation of sediment core GeoB12312-3, PANGAEA, doi:10.1594/PANGAEA.737532, 2010c.

Boudreau, B. P.: Mathematics of tracer mixing in sediments; II, Nonlocal mixing and biological conveyor-belt phenomena, Am. J. Sci., 286(3), 199–238, doi:10.2475/ajs.286.3.199, 1986.

Boudreau, B. P.: Is burial velocity a master parameter for bioturbation?, Geochim. Cosmochim. Acta, 58(4), 1243–1249, doi:10.1016/0016-7037(94)90378-6, 1994.

Boudreau, B. P.: Diagenetic Models and Their Implementation: Modelling Transport and Reactions in Aquatic Sediments, Springer Berlin Heidelberg, Berlin, Heidelberg., 1997.

Boudreau, B. P.: Mean mixed depth of sediments: The wherefore and the why, Limnol. Oceanogr., 43(3), 524–526, doi:10.4319/lo.1998.43.3.0524, 1998.

Boudreau, B. P. and Ruddick, B. R.: On a reactive continuum representation of organic matter diagenesis, Am. J. Sci., 291(5), 507–538, doi:10.2475/ajs.291.5.507, 1991.

Bowles, M. W., Mogollon, J. M., Kasten, S., Zabel, M. and Hinrichs, K.-U.: Global rates of marine sulfate reduction and implications for sub-sea-floor metabolic activities, Science, 344(6186), 889–891, doi:10.1126/science.1249213, 2014.

Bradley, J. A., Arndt, S., Amend, J. P., Burwicz, E., Dale, A. W., Egger, M. and LaRowe, D. E.: Widespread energy limitation to life in global subseafloor sediments, Sci. Adv., 6(32), eaba0697, doi:10.1126/sciadv.aba0697, 2020.

Burdige, D. J.: Burial of terrestrial organic matter in marine sediments: A re-assessment, Glob. Biogeochem. Cycles, 19(4), 1–7, doi:10.1029/2004GB002368, 2005.

Burdige, D. J.: Geochemistry of marine sediments, Princeton University Press, Princeton, NJ., 2006.

Calliari, D., Brugnoli, E., Ferrari, G. and Vizziano, D.: Phytoplankton distribution and production along a wide environmental gradient in the South-West Atlantic off Uruguay, Hydrobiologia, 620(1), 47–61, doi:10.1007/s10750-008-9614-7, 2009.

Canfield, D. E., Jørgensen, B. B., Fossing, H., Glud, R., Gundersen, J., Ramsing, N. B., Thamdrup, B., Hansen, J. W., Nielsen, L. P. and Hall, P. O. J.: Pathways of organic carbon oxidation in three continental margin sediments, Mar. Geol., 113(1–2), 27–40, doi:10.1016/0025-3227(93)90147-N, 1993.

Carreto, J. I., Montoya, N. G., Benavides, H. R., Guerrero, R. and Carignan, M. O.: Characterization of spring phytoplankton communities in the Rio de La Plata maritime front using pigment signatures and cell microscopy, Mar. Biol., 143(5), 1013–1027, doi:10.1007/s00227-003-1147-z, 2003.

Cathalot, C., Rabouille, C., Pastor, L., Deflandre, B., Viollier, E., Buscail, R., Grémare, A., Treignier, C. and Pruski, A.: Temporal variability of carbon recycling in coastal sediments influenced by rivers: assessing the impact of flood inputs in the Rhône River prodelta, Biogeosciences, 7(3), 1187–1205, doi:10.5194/bg-7-1187-2010, 2010.

Chen, D. and Chen, H. W.: Using the Köppen classification to quantify climate variation and change: An example for 1901–2010, Environ. Dev., 6, 69–79, doi:10.1016/j.envdev.2013.03.007, 2013.

Chen, X., Andersen, T. J., Morono, Y., Inagaki, F., Jørgensen, B. B. and Lever, M. A.: Bioturbation as a key driver behind the dominance of Bacteria over Archaea in near-surface sediment, Sci. Rep., 7(1), 2400, doi:10.1038/s41598-017-02295-x, 2017.

Colombo, J. C., Silverberg, N. and Gearing, J. N.: Lipid biogeochemistry in the Laurentian Trough—II. Changes in composition of fatty acids, sterols and aliphatic hydrocarbons during early diagenesis, Org. Geochem., 26(3–4), 257–274, doi:10.1016/S0146-6380(96)00146-5, 1997.

Contreras, S., Meister, P., Liu, B., Prieto-Mollar, X., Hinrichs, K.-U., Khalili, A., Ferdelman, T. G., Kuypers, M. M. M. and Jorgensen, B. B.: Cyclic 100-ka (glacial-interglacial) migration of subseafloor redox zonation on the Peruvian shelf, Proc. Natl. Acad. Sci., 110(45), 18098–18103, doi:10.1073/pnas.1305981110, 2013.

Cowie, G.: The biogeochemistry of Arabian Sea surficial sediments: A review of recent studies, Prog. Oceanogr., 65(2–4), 260–289, doi:10.1016/j.pocean.2005.03.003, 2005.

Coyle, K. O., Pinchuk, A. I., Eisner, L. B. and Napp, J. M.: Zooplankton species composition, abundance and biomass on the eastern Bering Sea shelf during summer: The potential role of water-column stability and nutrients in structuring the zooplankton community, Deep Sea Res. Part II Top. Stud. Oceanogr., 55(16–17), 1775–1791, doi:10.1016/j.dsr2.2008.04.029, 2008.

Cram, J. A., Weber, T., Leung, S. W., McDonnell, A. M. P., Liang, J.-H. and Deutsch, C.: The Role of Particle Size, Ballast, Temperature, and Oxygen in the Sinking Flux to the Deep Sea, Glob. Biogeochem. Cycles, 32(5), 858–876, doi:10.1029/2017GB005710, 2018.

Dahl, E. and Johannessen, T.: Temporal and spatial variability of phytoplankton and chlorophyll a: lessons from the south coast of Norway and the Skagerrak, ICES J. Mar. Sci., 55(4), 680–687, doi:10.1006/jmsc.1998.0401, 1998.

Dai, J., Sun, M.-Y., Culp, R. A. and Noakes, J. E.: A laboratory study on biochemical degradation and microbial utilization of organic matter comprising a marine diatom, land grass, and salt marsh plant in estuarine ecosystems, Aquat. Ecol., 43(4), 825–841, doi:10.1007/s10452-008-9211-x, 2009.

Dale, A. W., Regnier, P., Knab, N. J., Jørgensen, B. B. and Van Cappellen, P.: Anaerobic oxidation of methane (AOM) in marine sediments from the Skagerrak (Denmark): II. Reaction-transport modeling, Geochim. Cosmochim. Acta, 72(12), 2880–2894, doi:10.1016/j.gca.2007.11.039, 2008a.

Dale, A. W., Aguilera, D. R., Regnier, P., Fossing, H., Knab, N. J. and Jørgensen, B. B.: Seasonal dynamics of the depth and rate of anaerobic oxidation of methane in Aarhus Bay (Denmark) sediments, J. Mar. Res., 66(1), 127–155, doi:10.1357/002224008784815775, 2008b.

Dale, A. W., Brüchert, V., Alperin, M. and Regnier, P.: An integrated sulfur isotope model for Namibian shelf sediments, Geochim. Cosmochim. Acta, 73(7), 1924–1944, doi:10.1016/j.gca.2008.12.015, 2009.

Dale, A. W., Sommer, S., Bohlen, L., Treude, T., Bertics, V. J., Bange, H. W., Pfannkuche, O., Schorp, T., Mattsdotter, M. and Wallmann, K.: Rates and regulation of nitrogen cycling in seasonally hypoxic sediments during winter (Boknis Eck, SW Baltic Sea): Sensitivity to environmental variables, Estuar. Coast. Shelf Sci., 95(1), 14–28, doi:10.1016/j.ecss.2011.05.016, 2011.

Dale, A. W., Nickelsen, L., Scholz, F., Hensen, C., Oschlies, A. and Wallmann, K.: A revised global estimate of dissolved iron fluxes from marine sediments, Glob. Biogeochem. Cycles, 29(5), 691–707, doi:10.1002/2014GB005017, 2015.

Dale, A. W., Flury, S., Fossing, H., Regnier, P., Røy, H., Scholze, C. and Jørgensen, B. B.: Kinetics of organic carbon mineralization and methane formation in marine sediments (Aarhus Bay, Denmark), Geochim. Cosmochim. Acta, 252, 159–178, doi:10.1016/j.gca.2019.02.033, 2019.

Dauwe, B., Middelburg, J. J., Van Rijswijk, P., Sinke, J., Herman, P. M. J. and Heip, C. H. R.: Enzymatically hydrolyzable amino acids in North Sea sediments and their possible implication for sediment nutritional values, J. Mar. Res., 57(1), 109–134, doi:10.1357/002224099765038580, 1999a.

Dauwe, B., Middelburg, J. J., Herman, P. M. J. and Heip, C. H. R.: Linking diagenetic alteration of amino acids and bulk organic matter reactivity, Limnol. Oceanogr., 44(7), 1809–1814, doi:10.4319/lo.1999.44.7.1809, 1999b.

Dumoulin, J.-P., Pozzato, L., Rassman, J., Toussaint, F., Fontugne, M., Tisnérat-Laborde, N., Beck, L., Caffy, I., Delqué-Količ, E., Moreau, C. and Rabouille, C.: Isotopic Signature ($\delta^{13}C$, $\Delta^{14}C$) of DIC in Sediment Pore Waters: An Example from the Rhone River Delta, Radiocarbon, 60(5), 1465–1481, doi:10.1017/RDC.2018.111, 2018.

Dyer, K. R.: Sedimentation processes in the Bristol Channel/Severn Estuary, Mar. Pollut. Bull., 15(2), 53–57, doi:10.1016/0025-326X(84)90462-4, 1984.

Egger, M., Riedinger, N., Mogollón, J. M. and Jørgensen, B. B.: Global diffusive fluxes of methane in marine sediments, Nat. Geosci., 11(6), 421–425, doi:10.1038/s41561-018-0122-8, 2018.

Emerson, S. and Hedges, J. I.: Processes controlling the organic carbon content of open ocean sediments, Paleoceanography, 3(5), 621–634, doi:10.1029/PA003i005p00621, 1988.

Epping, E., van der Zee, C., Soetaert, K. and Helder, W.: On the oxidation and burial of organic carbon in sediments of the Iberian margin and Nazaré Canyon (NE Atlantic), Prog. Oceanogr., 52(2–4), 399–431, doi:10.1016/S0079-6611(02)00017-4, 2002.

Faust, J. C., Stevenson, M. A., Abbott, G. D., Knies, J., Tessin, A. C., Mannion, I., Ford, A., Hilton, R. G., Peakall, J. and März, C.: Does Arctic warming reduce preservation of organic matter in Barents Sea sediments?, Phil. Trans. R. Soc. A., 378, 1–18, doi:https://doi.org/10.1098/rsta.2019.0364, 2020.

Findlay, A. J., Pellerin, A., Laufer, K. and Jørgensen, B. B.: Quantification of sulphide oxidation rates in marine sediment, Geochim. Cosmochim. Acta, 280, 441–452, doi:10.1016/j.gca.2020.04.007, 2020.

Fischer, D., Sahling, H., Nöthen, K., Bohrmann, G., Zabel, M. and Kasten, S.: Interaction between hydrocarbon seepage, chemosynthetic communities, and bottom water redox at cold seeps of the Makran accretionary prism: insights from habitat-specific pore water sampling and modeling, Biogeosciences, 9(6), 2013–2031, doi:10.5194/bg-9-2013-2012, 2012.

Fleming, V. and Kaitala, S.: Phytoplankton Spring Bloom Intensity Index for the Baltic Sea Estimated for the years 1992 to 2004, Hydrobiologia, 554(1), 57–65, doi:10.1007/s10750-005-1006-7, 2006.

Fleming-Lehtinen, V. and Laamanen, M.: Long-term changes in Secchi depth and the role of phytoplankton in explaining light attenuation in the Baltic Sea, Estuar. Coast. Shelf Sci., 102–103, 1–10, doi:10.1016/j.ecss.2012.02.015, 2012.

Flury, S., Røy, H., Dale, A. W., Fossing, H., Tóth, Z., Spiess, V., Jensen, J. B. and Jørgensen, B. B.: Controls on subsurface methane fluxes and shallow gas formation in Baltic Sea sediment (Aarhus Bay, Denmark), Geochim. Cosmochim. Acta, 188, 297–309, doi:10.1016/j.gca.2016.05.037, 2016.

Freitas, F. S., Hendry, K. R., Henley, S. F., Faust, J. C., Tessin, A. C., Stevenson, M. A., Abbott, G. D., März, C. and Arndt, S.: Benthic-pelagic coupling in the Barents Sea: an integrated data-model framework, Phil. Trans. R. Soc. A., 378, 1–15, doi:http://dx.doi.org/10.1098/rsta.2019.0359, 2020.

Gayoso, A. M.: Bloom of Emiliania huxleyi (Prymnesiophyceae) in the western South Atlantic Ocean, J. Plankton Res., 17(8), 1717–1722, doi:10.1093/plankt/17.8.1717, 1995.

Gersonde, R.: The expedition of the research vessel “Sonne” to the subpolar North Pacific and the Bering Sea in 2009 (SO202-INOPEX) (Reports on polar and marine research No. 643), Alfred Wegener Institute for Polar and Marine Research, Bremerhaven., 2009.

Glud, R. N.: Oxygen dynamics of marine sediments, Mar. Biol. Res., 4(4), 243–289, doi:10.1080/17451000801888726, 2008.

Griffith, D. R., Martin, W. R. and Eglinton, T. I.: The radiocarbon age of organic carbon in marine surface sediments, Geochim. Cosmochim. Acta, 74(23), 6788–6800, doi:10.1016/j.gca.2010.09.001, 2010.

Grossi, V., Caradec, S. and Gilbert, F.: Burial and reactivity of sedimentary microalgal lipids in bioturbated Mediterranean coastal sediments, Mar. Chem., 81(1–2), 57–69, doi:10.1016/S0304-4203(02)00139-1, 2003.

de Haas, H. and van Weering, T. C. E.: Recent sediment accumulation, organic carbon burial and transport in the northeastern North Sea, Mar. Geol., 136(3–4), 173–187, doi:10.1016/S0025-3227(96)00072-2, 1997.

Hartnett, H. E., Keil, R. G., Hedges, J. I. and Devol, A. H.: Influence of oxygen exposure time on organic carbon preservation in continental margin sediments, Nature, 391(6667), 572–575, doi:10.1038/35351, 1998.

Havskum, H. and Riemann, B.: Ecological importance of bacterivorous, pigmented flagellates (mixotrophs) in the Bay of Aarhus, Denmark, Mar. Ecol. Prog. Ser., 137, 251–263, doi:10.3354/meps137251, 1996.

Hebbeln, D., Scheurle, C. and Lamy, F.: Depositional history of the Helgoland mud area, German Bight, North Sea, Geo-Mar. Lett., 23(2), 81–90, doi:10.1007/s00367-003-0127-0, 2003.

Hedges, J. I.: Global biogeochemical cycles: progress and problems, Mar. Chem., 39(1–3), 67–93, doi:10.1016/0304-4203(92)90096-S, 1992.

Hedges, J. I. and Oades, J. M.: Comparative organic geochemistries of soils and marine sediments, Org. Geochem., 27(7–8), 319–361, doi:10.1016/S0146-6380(97)00056-9, 1997.

Hedges, J. I., Keil, R. G. and Benner, R.: What happens to terrestrial organic matter in the ocean?, Org. Geochem., 27(5–6), 195–212, doi:10.1016/S0146-6380(97)00066-1, 1997.

Hemingway, J. D., Rothman, D. H., Grant, K. E., Rosengard, S. Z., Eglinton, T. I., Derry, L. A. and Galy, V. V.: Mineral protection regulates long-term global preservation of natural organic carbon, Nature, 570(7760), 228–231, doi:10.1038/s41586-019-1280-6, 2019.

Henkel, S. and Kulkarni, A.: Documentation of sediment core HE443/10-3, PANGAEA, doi:10.1594/PANGAEA.855884, 2015.

Henkel, S., Strasser, M., Schwenk, T., Hanebuth, T. J. J., Hüsener, J., Arnold, G. L., Winkelmann, D., Formolo, M., Tomasini, J., Krastel, S. and Kasten, S.: An interdisciplinary investigation of a recent submarine mass transport deposit at the continental margin off Uruguay, Geochem. Geophys. Geosystems, 12(8), 1–19, doi:10.1029/2011GC003669, 2011.

Henkel, S., Mogollón, J. M., Nöthen, K., Franke, C., Bogus, K., Robin, E., Bahr, A., Blumenberg, M., Pape, T., Seifert, R., März, C., de Lange, G. J. and Kasten, S.: Diagenetic barium cycling in Black Sea sediments – A case study for anoxic marine environments, Geochim. Cosmochim. Acta, 88, 88–105, doi:10.1016/j.gca.2012.04.021, 2012.

Henrichs, S. M.: Early diagenesis of organic matter in marine sediments: progress and perplexity, Mar. Chem., 39(1–3), 119–149, doi:10.1016/0304-4203(92)90098-U, 1992.

Hensen, C., Zabel, M. and Schulz, H. D.: A comparison of benthic nutrient fluxes from deep-sea sediments off Namibia and Argentina, Deep Sea Res. Part II Top. Stud. Oceanogr., 47(9), 2029–2050, doi:10.1016/S0967-0645(00)00015-1, 2000.

Hensen, C., Zabel, M., Pfeifer, K., Schwenk, T., Kasten, S., Riedinger, N., Schulz, H. D. and Boetius, A.: Control of sulfate pore-water profiles by sedimentary events and the significance of anaerobic oxidation of methane for the burial of sulfur in marine sediments, Geochim. Cosmochim. Acta, 67(14), 2631–2647, doi:10.1016/S0016-7037(03)00199-6, 2003.

Hensen, C., Zabel, M. and Schulz, H. N.: Benthic Cycling of Oxygen, Nitrogen and Phosphorus, in Marine Geochemistry, edited by H. D. Schulz and M. Zabel, pp. 207–240, Springer-Verlag, Berlin/Heidelberg., 2006.

Hickel, W., Berg, J. and Treutner, K.: Variability in phytoplankton biomass in the German Bight near Helgoland, in ICES Mar Sci Symp, vol. 195, pp. 249–259., 1992.

Hilligsøe, K. M., Jensen, J. B., Ferdelman, T. G., Fossing, H., Lapham, L., Røy, H. and Jørgensen, B. B.: Methane fluxes in marine sediments quantified through core analyses and seismo-acoustic mapping (Bornholm Basin, Baltic Sea), Geochim. Cosmochim. Acta, 239, 255–274, doi:10.1016/j.gca.2018.07.040, 2018.

Ho, T. C. and Aris, R.: On apparent second-order kinetics, AIChE J., 33(6), 1050–1051, doi:10.1002/aic.690330621, 1987.

Hoefs, M. J. L., Rijpstra, W. I. C. and Sinninghe Damsté, J. S.: The influence of oxic degradation on the sedimentary biomarker record I: evidence from Madeira Abyssal Plain turbidites, Geochim. Cosmochim. Acta, 66(15), 2719–2735, doi:10.1016/S0016-7037(02)00864-5, 2002.

Huguet, C., de Lange, G. J., Gustafsson, Ö., Middelburg, J. J., Sinninghe Damsté, J. S. and Schouten, S.: Selective preservation of soil organic matter in oxidized marine sediments (Madeira Abyssal Plain), Geochim. Cosmochim. Acta, 72(24), 6061–6068, doi:10.1016/j.gca.2008.09.021, 2008.

Hülse, D., Arndt, S., Daines, S., Regnier, P. and Ridgwell, A.: OMEN-SED 0.9: A novel, numerically efficient organic mattersediment diagenesis module for coupling to Earth system models, preprint, Climate and Earth System Modeling., 2018.

Hülse, D., Arndt, S. and Ridgwell, A.: Mitigation of Extreme Ocean Anoxic Event Conditions by Organic Matter Sulfurization, Paleoceanogr. Paleoclimatology, 34(4), 476–489, doi:10.1029/2018PA003470, 2019.

Jensen, M., Lomstein, E. and Sørensen, J.: Benthic NH4+ and NO3- flux following sedimentation of a spring phytoplankton bloom in Aarhus Bight, Denmark, Mar. Ecol. Prog. Ser., 61, 87–96, doi:10.3354/meps061087, 1990.

Jonas, P. J. C. and Millward, G. E.: Metals and nutrients in the Severn Estuary and Bristol Channel: Contemporary inputs and distributions, Mar. Pollut. Bull., 61(1–3), 52–67, doi:10.1016/j.marpolbul.2009.12.013, 2010.

Jørgensen, B. B.: A comparison of methods for the quantification of bacterial sulfate reduction in coastal marine sediments: II. Calculation from mathematical models, Geomicrobiol. J., 1(1), 29–47, doi:10.1080/01490457809377722, 1978.

Jørgensen, B. B. and Kasten, S.: Sulfur Cycling and Methane Oxidation, in Marine Geochemistry, edited by H. D. Schulz and M. Zabel, pp. 271–309, Springer-Verlag, Berlin/Heidelberg., 2006.

Jørgensen, B. B., Beulig, F., Egger, M., Petro, C., Scholze, C. and Røy, H.: Organoclastic sulfate reduction in the sulfate-methane transition of marine sediments, Geochim. Cosmochim. Acta, 254, 231–245, doi:10.1016/j.gca.2019.03.016, 2019a.

Jørgensen, B. B., Findlay, A. J. and Pellerin, A.: The Biogeochemical Sulfur Cycle of Marine Sediments, Front. Microbiol., 10, 849, doi:10.3389/fmicb.2019.00849, 2019b.

Jourabchi, P.: Quantitative interpretation of pH distributions in aquatic sediments: A reaction-transport modeling approach, Am. J. Sci., 305(9), 919–956, doi:10.2475/ajs.305.9.919, 2005.

Karlson, B., Edler, L., Granéli, W., Sahlsten, E. and Kuylenstierna, M.: Subsurface chlorophyll maxima in the Skagerrak-processes and plankton community structure, J. Sea Res., 35(1–3), 139–158, doi:10.1016/S1385-1101(96)90742-X, 1996.

Kayler, Z. E., Premke, K., Gessler, A., Gessner, M. O., Griebler, C., Hilt, S., Klemedtsson, L., Kuzyakov, Y., Reichstein, M., Siemens, J., Totsche, K.-U., Tranvik, L., Wagner, A., Weitere, M. and Grossart, H.-P.: Integrating Aquatic and Terrestrial Perspectives to Improve Insights Into Organic Matter Cycling at the Landscape Scale, Front. Earth Sci., 7, 127, doi:10.3389/feart.2019.00127, 2019.

Keil, R. G. and Cowie, G. L.: Organic matter preservation through the oxygen-deficient zone of the NE Arabian Sea as discerned by organic carbon:mineral surface area ratios, Mar. Geol., 161(1), 13–22, doi:10.1016/S0025-3227(99)00052-3, 1999.

Knab, N. J., Cragg, B. A., Borowski, C., Parkes, R. J., Pancost, R. and Jørgensen, B. B.: Anaerobic oxidation of methane (AOM) in marine sediments from the Skagerrak (Denmark): I. Geochemical and microbiological analyses, Geochim. Cosmochim. Acta, 72(12), 2868–2879, doi:10.1016/j.gca.2008.03.016, 2008.

Koho, K. A., Nierop, K. G. J., Moodley, L., Middelburg, J. J., Pozzato, L., Soetaert, K., van der Plicht, J. and Reichart, G.-J.: Microbial bioavailability regulates organic matter preservation in marine sediments, Biogeosciences, 10(2), 1131–1141, doi:10.5194/bg-10-1131-2013, 2013.

Krumins, V., Gehlen, M., Arndt, S., Van Cappellen, P. and Regnier, P.: Dissolved inorganic carbon and alkalinity fluxes from coastal marine sediments: model estimates for different shelf environments and sensitivity to global change, Biogeosciences, 10(1), 371–398, doi:10.5194/bg-10-371-2013, 2013.

Langston, W. J., Pope, N. D., Jonas, P. J. C., Nikitic, C., Field, M. D. R., Dowell, B., Shillabeer, N., Swarbrick, R. H. and Brown, A. R.: Contaminants in fine sediments and their consequences for biota of the Severn Estuary, Mar. Pollut. Bull., 61(1–3), 68–82, doi:10.1016/j.marpolbul.2009.12.014, 2010.

LaRowe, D. E., Arndt, S., Bradley, J. A., Burwicz, E., Dale, A. W. and Amend, J. P.: Organic carbon and microbial activity in marine sediments on a global scale throughout the Quaternary, Geochim. Cosmochim. Acta, 286, 227–247, doi:10.1016/j.gca.2020.07.017, 2020a.

LaRowe, D. E., Arndt, S., Bradley, J. A., Estes, E. R., Hoarfrost, A., Lang, S. Q., Lloyd, K. G., Mahmoudi, N., Orsi, W. D., Shah Walter, S. R., Steen, A. D. and Zhao, R.: The fate of organic carbon in marine sediments - New insights from recent data and analysis, Earth-Sci. Rev., 204, 103146, doi:10.1016/j.earscirev.2020.103146, 2020b.

Latasa, M. and Bidigare, R. R.: A comparison of phytoplankton populations of the Arabian Sea during the Spring Intermonsoon and Southwest Monsoon of 1995 as described by HPLC-analyzed pigments, Deep Sea Res. Part II Top. Stud. Oceanogr., 45(10–11), 2133–2170, doi:10.1016/S0967-0645(98)00066-6, 1998.

Lengger, S. K., Rush, D., Mayser, J. P., Blewett, J., Schwartz-Narbonne, R., Talbot, H. M., Middelburg, J. J., Jetten, M. S. M., Schouten, S., Sinninghe Damsté, J. S. and Pancost, R. D.: Dark carbon fixation in the Arabian Sea oxygen minimum zone contributes to sedimentary organic carbon (SOM), Glob. Biogeochem. Cycles, 2019GB006282, doi:10.1029/2019GB006282, 2019.

Lessin, G., Artioli, Y., Almroth-Rosell, E., Blackford, J. C., Dale, A. W., Glud, R. N., Middelburg, J. J., Pastres, R., Queirós, A. M., Rabouille, C., Regnier, P., Soetaert, K., Solidoro, C., Stephens, N. and Yakushev, E.: Modelling Marine Sediment

Biogeochemistry: Current Knowledge Gaps, Challenges, and Some Methodological Advice for Advancement, Front. Mar. Sci., 5, 19, doi:10.3389/fmars.2018.00019, 2018.

Lohse, L., Malschaert, J. F. P., Slomp, C. P., Helder, W. and van Raaphorst, W.: Sediment-water fluxes of inorganic nitrogen compounds along the transport route of organic matter in the North Sea, Ophelia, 41(1), 173–197, doi:10.1080/00785236.1995.10422043, 1995.

Lomstein, E., Jensen, M. H. and Sørensen, J.: Intracellular NH4+ and NO3- pools associated with deposited phytoplankton in a marine sediment (Aarhus Bight, Denmark), Mar. Ecol. Prog. Ser., 61(1/2), 97–105, 1990.

Luff, R., Wallmann, K., Grandel, S. and Schlüter, M.: Numerical modeling of benthic processes in the deep Arabian Sea, Deep Sea Res. Part II Top. Stud. Oceanogr., 47(14), 3039–3072, doi:10.1016/S0967-0645(00)00058-8, 2000.

Łukawska-Matuszewska, K. and Graca, B.: Pore water alkalinity below the permanent halocline in the Gdańsk Deep (Baltic Sea) - Concentration variability and benthic fluxes, Mar. Chem., 204, 49–61, doi:10.1016/j.marchem.2018.05.011, 2018.

Ma, W.-W., Zhu, M.-X., Yang, G.-P. and Li, T.: Iron geochemistry and organic carbon preservation by iron (oxyhydr)oxides in surface sediments of the East China Sea and the south Yellow Sea, J. Mar. Syst., 178, 62–74, doi:10.1016/j.jmarsys.2017.10.009, 2018.

Maerz, J., Six, K. D., Stemmler, I., Ahmerkamp, S. and Ilyina, T.: Microstructure and composition of marine aggregates as co-determinants for vertical particulate organic carbon transfer in the global ocean, preprint, Earth System Science/Response to Global Change: Climate Change., 2019.

Manning, A. J., Langston, W. J. and Jonas, P. J. C.: A review of sediment dynamics in the Severn Estuary: Influence of flocculation, Mar. Pollut. Bull., 61(1–3), 37–51, doi:10.1016/j.marpolbul.2009.12.012, 2010.

Marquardt, M., Hensen, C., Piñero, E., Wallmann, K. and Haeckel, M.: A transfer function for the prediction of gas hydrate inventories in marine sediments, Biogeosciences, 7(9), 2925–2941, doi:10.5194/bg-7-2925-2010, 2010.

Mayer, L. M.: Relationships between mineral surfaces and organic carbon concentrations in soils and sediments, Chem. Geol., 114(3–4), 347–363, doi:10.1016/0009-2541(94)90063-9, 1994a.

Mayer, L. M.: Surface area control of organic carbon accumulation in continental shelf sediments, Geochim. Cosmochim. Acta, 58(4), 1271–1284, doi:10.1016/0016-7037(94)90381-6, 1994b.

Mayer, L. M.: Sedimentary organic matter preservation: an assessment and speculative synthesis—a comment, Mar. Chem., 49(2–3), 123–126, doi:10.1016/0304-4203(95)00011-F, 1995.

Meile, C. and Van Cappellen, P.: Particle age distributions and O_2 exposure times: Timescales in bioturbated sediments, Glob. Biogeochem. Cycles, 19(3), 1–12, doi:10.1029/2004GB002371, 2005.

Meister, P., Liu, B., Ferdelman, T. G., Jørgensen, B. B. and Khalili, A.: Control of sulphate and methane distributions in marine sediments by organic matter reactivity, Geochim. Cosmochim. Acta, 104, 183–193, doi:10.1016/j.gca.2012.11.011, 2013.

Mewes, K., Mogollón, J. M., Picard, A., Rühlemann, C., Kuhn, T., Nöthen, K. and Kasten, S.: Impact of depositional and biogeochemical processes on small scale variations in nodule abundance in the Clarion-Clipperton Fracture Zone, Deep Sea Res. Part Oceanogr. Res. Pap., 91, 125–141, doi:10.1016/j.dsr.2014.06.001, 2014.

https://doi.org/10.5194/bg-2020-435
Preprint. Discussion started: 6 January 2021

Mewes, K., Mogollón, J. M., Picard, A., Rühlemann, C., Eisenhauer, A., Kuhn, T., Ziebis, W. and Kasten, S.: Diffusive transfer of oxygen from seamount basaltic crust into overlying sediments: An example from the Clarion–Clipperton Fracture Zone, Earth Planet. Sci. Lett., 433, 215–225, doi:10.1016/j.epsl.2015.10.028, 2016.

Meyers, P. A.: Organic geochemical proxies of paleoceanographic, paleolimnologic, and paleoclimatic processes, Org. Geochem., 27(5–6), 213–250, doi:10.1016/S0146-6380(97)00049-1, 1997.

Middelburg, J. J.: A simple rate model for organic matter decomposition in marine sediments, Geochim. Cosmochim. Acta, 53(7), 1577–1581, doi:10.1016/0016-7037(89)90239-1, 1989.

Middelburg, J. J.: Reviews and syntheses: to the bottom of carbon processing at the seafloor, Biogeosciences, 15(2), 413–427, doi:10.5194/bg-15-413-2018, 2018.

Middelburg, J. J.: Marine Carbon Biogeochemistry: A Primer for Earth System Scientists, Springer International Publishing, Cham., 2019.

Middelburg, J. J., Vlug, T., Jaco, F. and van der Nat, W. A.: Organic matter mineralization in marine systems, Glob. Planet. Change, 8(1–2), 47–58, doi:10.1016/0921-8181(93)90062-S, 1993.

Middelburg, J. J., Soetaert, K. and Herman, P. M. J.: Empirical relationships for use in global diagenetic models, Deep Sea Res. Part Oceanogr. Res. Pap., 44(2), 327–344, doi:10.1016/S0967-0637(96)00101-X, 1997.

Mogollón, J. M., Dale, A. W., Fossing, H. and Regnier, P.: Timescales for the development of methanogenesis and free gas layers in recently-deposited sediments of Arkona Basin (Baltic Sea), Biogeosciences, 9(5), 1915–1933, doi:10.5194/bg-9-1915-2012, 2012.

Mogollón, J. M., Mewes, K. and Kasten, S.: Quantifying manganese and nitrogen cycle coupling in manganese-rich, organic carbon-starved marine sediments: Examples from the Clarion-Clipperton fracture zone, Geophys. Res. Lett., 43(13), 7114–7123, doi:10.1002/2016GL069117, 2016.

Mollenhauer, G., Eglinton, T. I., Ohkouchi, N., Schneider, R. R., Müller, P. J., Grootes, P. M. and Rullkötter, J.: Asynchronous alkenone and foraminifera records from the Benguela Upwelling System, Geochim. Cosmochim. Acta, 67(12), 2157–2171, doi:10.1016/S0016-7037(03)00168-6, 2003.

Mollenhauer, G., McManus, J. F., Benthien, A., Müller, P. J. and Eglinton, T. I.: Rapid lateral particle transport in the Argentine Basin: Molecular 14C and 230Thxs evidence, Deep Sea Res. Part Oceanogr. Res. Pap., 53(7), 1224–1243, doi:10.1016/j.dsr.2006.05.005, 2006.

Mollenhauer, G., Inthorn, M., Vogt, T., Zabel, M., Sinninghe Damsté, J. S. and Eglinton, T. I.: Aging of marine organic matter during cross-shelf lateral transport in the Benguela upwelling system revealed by compound-specific radiocarbon dating, Geochem. Geophys. Geosystems, 8(9), 1–16, doi:10.1029/2007GC001603, 2007.

Müller, P. J. and Suess, E.: Productivity, sedimentation rate, and sedimentary organic matter in the oceans—I. Organic carbon preservation, Deep Sea Res. Part Oceanogr. Res. Pap., 26(12), 1347–1362, doi:10.1016/0198-0149(79)90003-7, 1979.

Niewöhner, C., Hensen, C., Kasten, S., Zabel, M. and Schulz, H. D.: Deep Sulfate Reduction Completely Mediated by Anaerobic Methane Oxidation in Sediments of the Upwelling Area off Namibia, Geochim. Cosmochim. Acta, 62(3), 455–464, doi:10.1016/S0016-7037(98)00055-6, 1998.

https://doi.org/10.5194/bg-2020-435
Preprint. Discussion started: 6 January 2021

Nöthen, K. and Kasten, S.: Reconstructing changes in seep activity by means of pore water and solid phase Sr/Ca and Mg/Ca ratios in pockmark sediments of the Northern Congo Fan, Mar. Geol., 287(1–4), 1–13, doi:10.1016/j.margeo.2011.06.008, 2011.

Odate, T.: Abundance and size composition of the summer phytoplankton communities in the western North Pacific Ocean, the Bering Sea, and the Gulf of Alaska, J. Oceanogr., 52(3), 335–351, doi:10.1007/BF02235928, 1996.

Ohkouchi, N., Eglinton, T. I., Keigwin, L. D. and Hayes, J. M.: Spatial and Temporal Offsets Between Proxy Records in a Sediment Drift, Science, 298(5596), 1224, doi:10.1126/science.1075287, 2002.

Oni, O., Miyatake, T., Kasten, S., Richter-Heitmann, T., Fischer, D., Wagenknecht, L., Kulkarni, A., Blumers, M., Shylin, S. I., Ksenofontov, V., Costa, B. F. O., Klingelhöfer, G. and Friedrich, M. W.: Distinct microbial populations are tightly linked to the profile of dissolved iron in the methanic sediments of the Helgoland mud area, North Sea, Front. Microbiol., 06, doi:10.3389/fmicb.2015.00365, 2015a.

Oni, O. E., Schmidt, F., Miyatake, T., Kasten, S., Witt, M., Hinrichs, K.-U. and Friedrich, M. W.: Microbial Communities and Organic Matter Composition in Surface and Subsurface Sediments of the Helgoland Mud Area, North Sea, Front. Microbiol., 6, doi:10.3389/fmicb.2015.01290, 2015b.

Paraska, D. W., Hipsey, M. R. and Salmon, S. U.: Sediment diagenesis models: Review of approaches, challenges and opportunities, Environ. Model. Softw., 61, 297–325, doi:10.1016/j.envsoft.2014.05.011, 2014.

Pastor, L., Deflandre, B., Viollier, E., Cathalot, C., Metzger, E., Rabouille, C., Escoubeyrou, K., Lloret, E., Pruski, A. M., Vétion, G., Desmalades, M., Buscail, R. and Grémare, A.: Influence of the organic matter composition on benthic oxygen demand in the Rhône River prodelta (NW Mediterranean Sea), Cont. Shelf Res., 31(9), 1008–1019, doi:10.1016/j.csr.2011.03.007, 2011.

Peterson, R. G.: The boundary currents in the western Argentine Basin, Deep Sea Res. Part Oceanogr. Res. Pap., 39(3–4), 623–644, doi:10.1016/0198-0149(92)90092-8, 1992.

Pierre, C. and Fouquet, Y.: Authigenic carbonates from methane seeps of the Congo deep-sea fan, Geo-Mar. Lett., 27(2–4), 249–257, doi:10.1007/s00367-007-0081-3, 2007.

Pozzato, L., Rassmann, J., Lansard, B., Dumoulin, J.-P., van Breugel, P. and Rabouille, C.: Origin of remineralized organic matter in sediments from the Rhone River prodelta (NW Mediterranean) traced by Δ 14 C and δ 13 C signatures of pore water DIC, Prog. Oceanogr., 163, 112–122, doi:10.1016/j.pocean.2017.05.008, 2018.

Premuzic, E. T., Benkovitz, C. M., Gaffney, J. S. and Walsh, J. J.: The nature and distribution of organic matter in the surface sediments of world oceans and seas, Org. Geochem., 4(2), 63–77, doi:10.1016/0146-6380(82)90009-2, 1982.

Pruski, A. M., Buscail, R., Bourgeois, S., Vétion, G., Coston-Guarini, J. and Rabouille, C.: Biogeochemistry of fatty acids in a river-dominated Mediterranean ecosystem (Rhône River prodelta, Gulf of Lions, France): Origins and diagenesis, Org. Geochem., 83–84, 227–240, doi:10.1016/j.orggeochem.2015.04.002, 2015.

Puglini, M., Brovkin, V., Regnier, P. and Arndt, S.: Assessing the potential for non-turbulent methane escape from the East Siberian Arctic Shelf, Biogeosciences, 17(12), 3247–3275, doi:10.5194/bg-17-3247-2020, 2020.

Rassmann, J., Lansard, B., Pozzato, L. and Rabouille, C.: Carbonate chemistry in sediment porewaters of the Rhône River deltadriven by early diagenesis (northwestern Mediterranean), Biogeosciences, 13(18), 5379–5394, doi:10.5194/bg-13-5379-2016, 2016.

Rassmann, J., Eitel, E. M., Lansard, B., Cathalot, C., Brandily, C., Taillefert, M. and Rabouille, C.: Benthic alkalinity and dissolved inorganic carbon fluxes in the Rhône River prodelta generated by decoupled aerobic and anaerobic processes, Biogeosciences, 17(1), 13–33, doi:10.5194/bg-17-13-2020, 2020.

Redfield, A. C.: On the proportions of organic derivatives in sea water and their relation to the composition of plankton, in James Johnstone Memorial Volume, pp. 176–192, University Press of Liverpool., 1934.

Regnier, P., Mouchet, A., Wollast, R. and Ronday, F.: A discussion of methods for estimating residual fluxes in strong tidal estuaries, Cont. Shelf Res., 18(13), 1543–1571, doi:10.1016/S0278-4343(98)00071-5, 1998.

Regnier, P., O'Kane, J. P., Steefel, C. I. and Vanderborght, J. P.: Modeling complex multi-component reactive-transport systems: towards a simulation environment based on the concept of a Knowledge Base, Appl. Math. Model., 26(9), 913–927, doi:10.1016/S0307-904X(02)00047-1, 2002.

Regnier, P., Dale, A. W., Arndt, S., LaRowe, D. E., Mogollón, J. and Van Cappellen, P.: Quantitative analysis of anaerobic oxidation of methane (AOM) in marine sediments: A modeling perspective, Earth-Sci. Rev., 106(1–2), 105–130, doi:10.1016/j.earscirev.2011.01.002, 2011.

Richardson, K., Rasmussen, B., Bunk, T. and Mouritsen, L. T.: Multiple subsurface phytoplankton blooms occurring simultaneously in the Skagerrak, J. Plankton Res., 25(7), 799–813, doi:10.1093/plankt/25.7.799, 2003.

Riebesell, U.: Aggregation of Phaeocystis during phytoplankton spring blooms in the southern North Sea, Mar. Ecol. Prog. Ser., 96(3), 281–289, 1993.

Riedinger, N., Pfeifer, K., Kasten, S., Garming, J. F. L., Vogt, C. and Hensen, C.: Diagenetic Alteration of Magnetic Signals by Anaerobic Oxidation of Methane Related to a Change in Sedimentation Rate, Geochim. Cosmochim. Acta, 69(16), 4117–4126, doi:10.1016/j.gca.2005.02.004, 2005.

Riedinger, N., Formolo, M. J., Lyons, T. W., Henkel, S., Beck, A. and Kasten, S.: An inorganic geochemical argument for coupled anaerobic oxidation of methane and iron reduction in marine sediments, Geobiology, 12(2), 172–181, doi:10.1111/gbi.12077, 2014.

Riedinger, N., Brunner, B., Krastel, S., Arnold, G. L., Wehrmann, L. M., Formolo, M. J., Beck, A., Bates, S. M., Henkel, S., Kasten, S. and Lyons, T. W.: Sulfur Cycling in an Iron Oxide-Dominated, Dynamic Marine Depositional System: The Argentine Continental Margin, Front. Earth Sci., 5, 33, doi:10.3389/feart.2017.00033, 2017.

Rixen, T., Gaye, B. and Emeis, K.-C.: The monsoon, carbon fluxes, and the organic carbon pump in the northern Indian Ocean, Prog. Oceanogr., 175, 24–39, doi:10.1016/j.pocean.2019.03.001, 2019.

Rysgaard, S., Fossing, H. and Jensen, M. M.: Organic matter degradation through oxygen respiration, denitrification, and manganese, iron, and sulfate reduction in marine sediments (the Kattegat and the Skagerrak), Ophelia, 55(2), 77–91, doi:10.1080/00785236.2001.10409475, 2001.

Salvadó, J. A., Tesi, T., Andersson, A., Ingri, J., Dudarev, O. V., Semiletov, I. P. and Gustafsson, Ö.: Organic carbon remobilized from thawing permafrost is resequestered by reactive iron on the Eurasian Arctic Shelf, Geophys. Res. Lett., 42(19), 8122–8130, doi:10.1002/2015GL066058, 2015.

Schlitzer, R.: Ocean data view., 2019.

Schulz, H. D., Dahmke, A., Schinzel, U., Wallmann, K. and Zabel, M.: Early diagenetic processes, fluxes, and reaction rates in sediments of the South Atlantic, Geochim. Cosmochim. Acta, 58(9), 2041–2060, doi:10.1016/0016-7037(94)90284-4, 1994.

Seiter, K., Hensen, C., Schröter, J. and Zabel, M.: Organic carbon content in surface sediments—defining regional provinces, Deep Sea Res. Part Oceanogr. Res. Pap., 51(12), 2001–2026, doi:10.1016/j.dsr.2004.06.014, 2004.

Seiter, K., Hensen, C. and Zabel, M.: Benthic carbon mineralization on a global scale, Glob. Biogeochem. Cycles, 19(1), 1–26, doi:10.1029/2004GB002225, 2005.

Shalapyonok, A., Olson, R. J. and Shalapyonok, L. S.: Arabian Sea phytoplankton during Southwest and Northeast Monsoons 1995: composition, size structure and biomass from individual cell properties measured by flow cytometry, Deep Sea Res. Part II Top. Stud. Oceanogr., 48(6–7), 1231–1261, doi:10.1016/S0967-0645(00)00137-5, 2001.

Shields, M. R., Bianchi, T. S., Gélinas, Y., Allison, M. A. and Twilley, R. R.: Enhanced terrestrial carbon preservation promoted by reactive iron in deltaic sediments, Geophys. Res. Lett., 43(3), 1149–1157, doi:10.1002/2015GL067388, 2016.

Sinninghe Damsté, J. S., Irene, W., Rijpstra, C., de Leeuw, J. W. and Schenck, P. A.: Origin of organic sulphur compounds and sulphur-containing high molecular weight substances in sediments and immature crude oils, Org. Geochem., 13(4–6), 593–606, doi:10.1016/0146-6380(88)90079-4, 1988.

Sinninghe Damsté, J. S., Kok, M. D., Köster, J. and Schouten, S.: Sulfurized carbohydrates: an important sedimentary sink for organic carbon?, Earth Planet. Sci. Lett., 164(1–2), 7–13, doi:10.1016/S0012-821X(98)00234-9, 1998.

Sinninghe Damsté, J. S., Rijpstra, W. I. C. and Reichart, G.: The influence of oxic degradation on the sedimentary biomarker record II. Evidence from Arabian Sea sediments, Geochim. Cosmochim. Acta, 66(15), 2737–2754, doi:10.1016/S0016-7037(02)00865-7, 2002.

Snyder, G. T., Hiruta, A., Matsumoto, R., Dickens, G. R., Tomaru, H., Takeuchi, R., Komatsubara, J., Ishida, Y. and Yu, H.: Pore water profiles and authigenic mineralization in shallow marine sediments above the methane-charged system on Umitaka Spur, Japan Sea, Deep Sea Res. Part II Top. Stud. Oceanogr., 54(11–13), 1216–1239, doi:10.1016/j.dsr2.2007.04.001, 2007.

Soetaert, K., Herman, P. M. J. and Middelburg, J. J.: A model of early diagenetic processes from the shelf to abyssal depths, Geochim. Cosmochim. Acta, 60(6), 1019–1040, doi:10.1016/0016-7037(96)00013-0, 1996.

Soetaert, K., Herman, P. M. J., Middelburg, J. J. and Heip, C.: Assessing organic matter mineralization, degradability and mixing rate in an ocean margin sediment (Northeast Atlantic) by diagenetic modeling, J. Mar. Res., 56(2), 519–534, doi:10.1357/002224098321822401, 1998.

Soetaert, K., Hofmann, A. F., Middelburg, J. J., Meysman, F. J. R. and Greenwood, J.: The effect of biogeochemical processes on pH, Mar. Chem., 105(1–2), 30–51, doi:10.1016/j.marchem.2006.12.012, 2007.

Stabeno, P. J. and Hunt, G. L.: Overview of the Inner Front and Southeast Bering Sea Carrying Capacity Programs, Deep Sea Res. Part II Top. Stud. Oceanogr., 49(26), 6157–6168, doi:10.1016/S0967-0645(02)00339-9, 2002.

Stockwell, D. A., Whitledge, T. E., Zeeman, S. I., Coyle, K. O., Napp, J. M., Brodeur, R. D., Pinchuk, A. I. and Hunt, G. L.: Anomalous conditions in the south-eastern Bering Sea, 1997: nutrients, phytoplankton and zooplankton, Fish. Oceanogr., 10(1), 99–116, doi:10.1046/j.1365-2419.2001.00158.x, 2001.

Stolpovsky, K., Dale, A. W. and Wallmann, K.: A new look at the multi-G model for organic carbon degradation in surface marine sediments for coupled benthic–pelagic simulations of the global ocean, Biogeosciences, 15(11), 3391–3407, doi:10.5194/bg-15-3391-2018, 2018.

Sun, M.-Y. and Wakeham, S. G.: Molecular evidence for degradation and preservation of organic matter in the anoxic Black Sea Basin, Geochim. Cosmochim. Acta, 58(16), 3395–3406, doi:10.1016/0016-7037(94)90094-9, 1994.

Sun, X. and Turchyn, A. V.: Significant contribution of authigenic carbonate to marine carbon burial, Nat. Geosci., 7(3), 201–204, doi:10.1038/ngeo2070, 2014.

Thamdrup, B., Fossing, H. and Jørgensen, B. B.: Manganese, iron and sulfur cycling in a coastal marine sediment, Aarhus bay, Denmark, Geochim. Cosmochim. Acta, 58(23), 5115–5129, doi:10.1016/0016-7037(94)90298-4, 1994.

Thingstad, T. F., Riemann, B., Havskum, H. and Garde, K.: Incorporation rates and biomass content of C and P in phytoplankton and bacteria in the Bay of Aarhus (Denmark) June 1992, J. Plankton Res., 18(1), 97–121, doi:10.1093/plankt/18.1.97, 1996.

Thomas, S.: The response of anaerobic prokaryotic processes and communities in the Severn Estuary sediments to environmental changes, Cardiff University, Cardiff., 2014.

Thullner, M., Dale, A. W. and Regnier, P.: Global-scale quantification of mineralization pathways in marine sediments: A reaction-transport modeling approach, Geochem. Geophys. Geosystems, 10(10), 1–24, doi:10.1029/2009GC002484, 2009.

Trimmer, M., Engström, P. and Thamdrup, B.: Stark Contrast in Denitrification and Anammox across the Deep Norwegian Trench in the Skagerrak, Appl. Environ. Microbiol., 79(23), 7381–7389, doi:10.1128/AEM.01970-13, 2013.

Tromp, T. K., Van Cappellen, P. and Key, R. M.: A global model for the early diagenesis of organic carbon and organic phosphorus in marine sediments, Geochim. Cosmochim. Acta, 59(7), 1259–1284, doi:10.1016/0016-7037(95)00042-X, 1995.

Uitz, J., Stramski, D., Gentili, B., D'Ortenzio, F. and Claustre, H.: Estimates of phytoplankton class-specific and total primary production in the Mediterranean Sea from satellite ocean color observations, Glob. Biogeochem. Cycles, 26(2), 1–10, doi:10.1029/2011GB004055, 2012.

Uncles, R. J.: Physical properties and processes in the Bristol Channel and Severn Estuary, Mar. Pollut. Bull., 61(1–3), 5–20, doi:10.1016/j.marpolbul.2009.12.010, 2010.

Underwood, G. J. C.: Microphytobenthos and phytoplankton in the Severn estuary, UK: Present situation and possible consequences of a tidal energy barrage, Mar. Pollut. Bull., 61(1–3), 83–91, doi:10.1016/j.marpolbul.2009.12.015, 2010.

Ussler, W. and Paull, C. K.: Rates of anaerobic oxidation of methane and authigenic carbonate mineralization in methane-rich deep-sea sediments inferred from models and geochemical profiles, Earth Planet. Sci. Lett., 266(3–4), 271–287, doi:10.1016/j.epsl.2007.10.056, 2008.

Van Cappellen, P. and Wang, Y.: Cycling of iron and manganese in surface sediments; a general theory for the coupled transport and reaction of carbon, oxygen, nitrogen, sulfur, iron, and manganese, Am. J. Sci., 296(3), 197–243, doi:10.2475/ajs.296.3.197, 1996.

Van Weering, T. C. E., Berger, G. W. and Kalf, J.: Recent sediment accumulation in the Skagerrak, Northeastern North Sea, Neth. J. Sea Res., 21(3), 177–189, doi:10.1016/0077-7579(87)90011-1, 1987.

Vandewiele, S., Cowie, G., Soetaert, K. and Middelburg, J. J.: Amino acid biogeochemistry and organic matter degradation state across the Pakistan margin oxygen minimum zone, Deep Sea Res. Part II Top. Stud. Oceanogr., 56(6–7), 376–392, doi:10.1016/j.dsr2.2008.05.035, 2009.

Volz, J. B., Mogollón, J. M., Geibert, W., Arbizu, P. M., Koschinsky, A. and Kasten, S.: Natural spatial variability of depositional conditions, biogeochemical processes and element fluxes in sediments of the eastern Clarion-Clipperton Zone, Pacific Ocean, Deep Sea Res. Part Oceanogr. Res. Pap., 140, 159–172, doi:10.1016/j.dsr.2018.08.006, 2018.

Wakeham, S. G., Lee, C., Hedges, J. I., Hernes, P. J. and Peterson, M. J.: Molecular indicators of diagenetic status in marine organic matter, Geochim. Cosmochim. Acta, 61(24), 5363–5369, doi:10.1016/S0016-7037(97)00312-8, 1997.

Wallmann, K., Aloisi, G., Haeckel, M., Obzhirov, A., Pavlova, G. and Tishchenko, P.: Kinetics of organic matter degradation, microbial methane generation, and gas hydrate formation in anoxic marine sediments, Geochim. Cosmochim. Acta, 70(15), 3905–3927, doi:10.1016/j.gca.2006.06.003, 2006.

Wang, D., Zhu, M.-X., Yang, G.-P. and Ma, W.-W.: Reactive Iron and Iron-Bound Organic Carbon in Surface Sediments of the River-Dominated Bohai Sea (China) Versus the Southern Yellow Sea, J. Geophys. Res. Biogeosciences, 124(1), 79–98, doi:10.1029/2018JG004722, 2019.

Wang, Y. and Van Cappellen, P.: A multicomponent reactive transport model of early diagenesis: Application to redox cycling in coastal marine sediments, Geochim. Cosmochim. Acta, 60(16), 2993–3014, doi:10.1016/0016-7037(96)00140-8, 1996.

Weber, T., Cram, J. A., Leung, S. W., DeVries, T. and Deutsch, C.: Deep ocean nutrients imply large latitudinal variation in particle transfer efficiency, Proc. Natl. Acad. Sci., 113(31), 8606–8611, doi:10.1073/pnas.1604414113, 2016.

Wehrmann, L. M., Arndt, S., März, C., Ferdelman, T. G. and Brunner, B.: The evolution of early diagenetic signals in Bering Sea subseafloor sediments in response to varying organic carbon deposition over the last 4.3Ma, Geochim. Cosmochim. Acta, 109, 175–196, doi:10.1016/j.gca.2013.01.025, 2013.

Westrich, J. T. and Berner, R. A.: The role of sedimentary organic matter in bacterial sulfate reduction: The *G* model tested, Limnol. Oceanogr., 29(2), 236–249, doi:10.4319/lo.1984.29.2.0236, 1984.

Wiltshire, K. H. and Manly, B. F. J.: The warming trend at Helgoland Roads, North Sea: phytoplankton response, Helgol. Mar. Res., 58(4), 269–273, doi:10.1007/s10152-004-0196-0, 2004.

Ye, H., Yang, T., Zhu, G., Jiang, S. and Wu, L.: Pore water geochemistry in shallow sediments from the northeastern continental slope of the South China sea, Mar. Pet. Geol., 75, 68–82, doi:10.1016/j.marpetgeo.2016.03.010, 2016.

Zebracki, M., Eyrolle-Boyer, F., Evrard, O., Claval, D., Mourier, B., Gairoard, S., Cagnat, X. and Antonelli, C.: Tracing the origin of suspended sediment in a large Mediterranean river by combining continuous river monitoring and measurement of artificial and natural radionuclides, Sci. Total Environ., 502, 122–132, doi:10.1016/j.scitotenv.2014.08.082, 2015.

Zettler, M. L., Schiedek, D. and Bobertz, B.: Benthic biodiversity indices versus salinity gradient in the southern Baltic Sea, Mar. Pollut. Bull., 55(1–6), 258–270, doi:10.1016/j.marpolbul.2006.08.024, 2007.

Zhou, C., Guan, C., Cui, H., Ouyang, Q. and Wang, W.: Methane-derived authigenic carbonate from the lower Doushantuo Formation of South China: Implications for seawater sulfate concentration and global carbon cycle in the early Ediacaran ocean, Palaeogeogr. Palaeoclimatol. Palaeoecol., 461, 145–155, doi:10.1016/j.palaeo.2016.08.017, 2016.

https://doi.org/10.5194/bg-2020-435
Preprint. Discussion started: 6 January 2021

Zonneveld, K. A. F., Versteegh, G. J. M., Kasten, S., Eglinton, T. I., Emeis, K.-C., Huguet, C., Koch, B. P., de Lange, G. J., de Leeuw, J. W., Middelburg, J. J., Mollenhauer, G., Prahl, F. G., Rethemeyer, J. and Wakeham, S. G.: Selective preservation of organic matter in marine environments; processes and impact on the sedimentary record, Biogeosciences, 7(2), 483–511, doi:10.5194/bg-7-483-2010, 2010.